AIMS Mathematics

https://www.aimspress.com/journal/Math

AIMS Mathematics, 11(8): 25265–25294.
DOI:10.3934/math.20261015
Received: 25 May 2026
Revised: 19 July 2026
Accepted: 27 July 2026
Published: 17 August 2026

Research article

Neural network adaptive optimized resilient event-triggered control for nonlinear systems

Jun Hu[1,*], **Wei Liu**[2,3] **and Shuai Cheng**[3]

[1] College of Software, Shenyang University of Technology, Shenyang 110870, China
[2] College of Computer Science and Engineering, Northeastern University, Shenyang 110819, China
[3] Neusoft Reach Automotive Technology (Shenyang) Co., Ltd., Shenyang 110179, China

* **Correspondence:** Email: hujun@sut.edu.cn.

Abstract: Considering an uncertain nonlinear system with unmeasurement states under denial-of-service (DoS) attacks, this paper presents an observer-based neural network (NN) adaptive optimal resilient event-triggered control (ETC) framework. First, the unknown dynamics of the system are approximated by neural networks (NNs), and therefore an NN state observer is developed to estimate the unmeasurable states of the system. Then, by introducing the hyperbolic tangent function and constructing an auxiliary variable, the adverse effect of the symmetric actuator saturation can be eliminated. Furthermore, an event-triggered (ET) mechanism is introduced to reduce controller update frequency and communication burden. During the reinforcemet learning algorithm, critic-actor NNs are employed to approximate the value function and control policy, respectively. Combining adaptive dynamic programming (ADP) and an adaptive backstepping technique, an adaptive event-triggered (ET) optimized secure control method is developed. According to the Lyapunov stability theory, all signals of the closed-loop system are proven as semi-globally uniformly ultimately bounded (SGUUB). Finally, the optimal resilient ETC control framework is utilized on a single-phase photovoltaic (PV) grid-connected power generation system, and the effectiveness of the investigated control approach is verified by simulation results.

Keywords: optimal control; nonlinear systems; coupled neural networks; DoS attacks; event-triggered control
Mathematics Subject Classification: 93C10, 93C40

1. Introduction

Nonlinear systems have received widespread concern from the scientific community, as they widely exist in electrical power, transportation, mechanical engineering, etc [1]. In order to address the complex control problem of nonlinear systems, scholars have investigated many intelligent control algorithms on the basis of NNs [2] and fuzzy logic systems (FLSs) [3, 4], and numerous relevant academic achievements have been obtained. By adopting the Lyapunov theory and the backstepping architecture, these approaches not only overcame the effects of unknown nonlinear dynamics, but could also guarantee that the system was ultimately stable. Specifically, the authors in [1] and [2] researched a kind of NN-based state constraints control scheme for the nonlinear system. Nevertheless, it should be noted that the results described above all suppose that the system states are completely accessible and could be employed straightforwardly to construct the state feedback controller.

To conquer the disadvantage of the state feedback control methodology that required all the state information of the system, observer-based NN or the FLS output feedback control techniques were widely studied [5]. At present, many valuable outcomes were published, such as those in [6–8]. The authors in [6] designed a state feedback controller and an output feedback controller for SISO nonlinear systems. Wang et al. [7] studied a tracking control issue for the MIMO nonlinear system with unmeasurable states. The work in [8] presented a fuzzy adaptive output feedback control scheme under the backstepping framework, in which the observer was used to obtain unmeasurable states. It should be pointed out that the network communication channels considered in the aforementioned works operate under normal conditions without cyberattacks. If their network communications were subject to cyber-attacks, the above-described approaches would not be able to ensure system stability.

To the best of our knowledge, due to the open character of the network environment, the system is easily subject to various attacks, which can diminish the performance of the system [9–11]. Hence, the security performance of the network layer is essential to guarantee reliable information transmission within the system [12–14]. Currently, there are three main categories of cyber-attacks: deception attacks [11], replay attacks [12], and DoS attacks [15–17]. In order to remove the negative impact of the DoS attack, the works in [13] and [14] researched an adaptive secure control strategy for interconnected large systems. Furthermore, Zhou and Tong [17] presented an observer-based fuzzy adaptive resilient formation control strategy for nonlinear multiagent systems under DoS attacks. However, the control approaches discussed in these papers did not involve control input saturation.

Actuator saturation easily occurs in the running process of the real system [18–20]. In particular, if the actuator has a saturation characteristic, the output will not change when the input reaches the upper limit [21, 22]. The mismatch between input and output implies the control signal cannot be fully executed by the actuator, and the actual control force fails to follow the designed control instruction. This will weaken or even destroy the stability of the system. In references [19, 23, 24], the hyperbolic tangent function was utilized to solve the symmetric input saturation problems. In [25] and [26], the Gaussian error function was employed to remove the adverse effects of asymmetric input saturation nonlinearities. A smooth nonlinear function was applied to estimate the saturated model, and a first-order auxiliary system was devised to compensate for the saturated nonlinearity in [27]. Zhang et al. [28] researched a tracking control issue for uncertain switched nonlinear systems, in which the Nussbaum function was adopted to overcome the saturated nonlinear problem. However, the control schemes investigated above did not consider the idea of optimal control, which means that their saturation controllers were not optimal. Fang et al. [29] studied the finite-time state tracking control issue for uncertain systems, in which a novel auxiliary system with a fractional-power term was designed to deal with the saturation nonlinearity.

As the core of contemporary control theory, optimization control is not only very significant in the field of nonlinear systems, but also has broad application prospects in practical industrial engineering. Furthermore, if control energy can be conserved while achieving optimized control, this will significantly improve the operational efficiency and practicality of the system. To obtain optimal performance, many scholars have incorporated event-triggered mechanisms based on optimal control. Nevertheless, the optimization control problem for nonlinear systems usually requires solving HJB equations, but the analytical solutions are difficult to obtain for this type of partial differential equation. For the purpose of eliminating the above deficiency, Bellman proposed the framework of dynamic programming. Nevertheless, expanding the variable dimensions will trigger a sharp surge in calculation volume, resulting in the notorious curse of dimensionality [30, 31]. Thus, the ADP and RL algorithms are proposed [32–34]. Specifically, Shen et al. [33] proposed an RL-based event-triggered optimal control approach via an identifier-critic-actor architecture for nonlinear servo systems. The work in [34] studied the prescribed performance robust attitude optimal control scheme for 2-DOF helicopters by using the reinforcement learning algorithm and a sliding mode switching strategy. In [35] and [36], the optimization ETC scheme was developed for heterogeneous vehicle platoon and multi-agent systems, respectively. The authors in [37] first constructed feedforward controllers by using the backstepping architecture, and subsequently designed an ADP-based optimal adaptive feedback controller for the converted affine nonlinear systems. Additionally, the work in [38] developed an ADP algorithm-based approximate optimized tracking control strategy, in which a steady-state and an optimization feedback controller were designed to achieve optimal control. On the other hand, to eliminate the issue of "complexity explosion" that arises during the backstepping optimization process, the work in [39] developed a kind of adaptive optimized output constraints dynamic surface control (DSC) scheme for the nonlinear systems.

Through the above theoretical analysis, this investigation presents the observer-based NN adaptive optimized secure ETC scheme for the nonlinear system with symmetric input saturated and DoS attacks.

The primary contributions can be outlined as follows:

1) In comparison with the control methods in [14] and [15] that do not consider the optimal performance function and communication overhead, an optimal ETC scheme is developed in this paper by combining the ET mechanism and the ADP algorithm via the critic-actor NNs, in which the communication constraints and the optimal control performance are balanced. Furthermore, the DSC technique is introduced to avoid computing the derivative of the optimal virtual control signal.

2) When the DoS attacks occur, the communication channel is interupted, leading to failed transmission of state information. To handle this situation, an NN state observer is designed in this paper to estimate the states of the system, which does not require such a priori knowledge. Compared to the normal information channel scenario considered in [27, 28, 31], this paper has a wider range of application scenarios.

3) Unlike [19, 23, 24], to eliminate the impact of the symmetric saturated nonlinearities link, a hyperbolic tangent function is utilized to approximate the symmetric saturation model, and a first-order auxiliary system is devised to compensate for the deviations of the control signal. Additionally, the NNs are applied to approximate unknown nonlinear dynamics. These drive the controlled system to become more practical in engineering applications, while simultaneously enhancing its robustness and adaptability.

2. Problem formulations and preliminaries

2.1. System description

Consider the uncertain strict feedback nonlinear system with form

$$\begin{aligned} \dot{x}_i &= c_i x_{i+1} + f_i(\bar{x}_i),\ i = 1, 2, 3, \cdots, n-1, \\ \dot{x}_n &= \kappa D(u(t)) + f_n(\bar{x}_n),\ n \geq 2, \\ y &= x_1, \end{aligned} \tag{2.1}$$

where $n > 0$, $c_i > 0$, and $\kappa > 0$ are constants. $\bar{x}_i = [x_1, x_2, x_3, ..., x_i]^T \in \mathbb{R}^i$ $(i = 1, 2, 3, \cdots, n)$ denotes the states vector. $D(u(t)) \in \mathbb{R}$ and $y \in \mathbb{R}$ denote the symmetric input with saturation and the output of the system, respectively. $f_i(\bar{x}_i)$ $(i = 1, 2, 3, ..., n)$ stand for the unknown functions. The system output y is assumed to be measurable. $D(u)$ satisfies the following piecewise function:

$$D(u) = \begin{cases} u^+_{sat}, & \text{if} \quad u > u^+_{sat}, \\ u, & \text{if}\ u^-_{sat} \leq u \leq u^+_{sat}, \\ u^-_{sat}, & \text{if} \quad u < u^-_{sat}, \end{cases} \tag{2.2}$$

where u indicates the actual control input of the system, and u^+_{sat} and u^-_{sat} represent the known upper and the lower limits of u, respectively.

Remark 1. Evidently, a sharp corner exists between the actual control input u and the applied control $D(u)$ when $u = u^+_{sat}$ and $u = u^-_{sat}$. Consequently, the traditional backstepping design approach [26] is not directly utilized in this paper.

In order to mitigate adverse effects caused by saturation nonlinearity, the hyperbolic tangent function $\tanh(u)$ is taken into account in place of the symmetric saturation model $D(u)$. Inevitably, there is a bounded error $\xi(t)$ between $\tanh(u)$ and $D(u)$, i.e.,

$$\xi(t) = -\tanh(u) + D(u). \tag{2.3}$$

By applying the mean-value theorem, (2.3) can be reformulated as

$$\tanh(u) = \tanh(u_0) + \frac{\partial \tanh(u)}{\partial u} |_{u=u^{\varsigma}} (u - u_0)\ , \tag{2.4}$$

where $u^{\varsigma} = \varsigma u + (1 - \varsigma) u_0$, $\varsigma \in (0, 1)$. Letting u_0 to be zero, (2.4) can be rewritten as

$$\tanh(u) = u(1 - \tanh^2(u^{\varsigma})). \tag{2.5}$$

As far as we know, all the signals of real systems are bounded. Hence, it is rational to assume that the control signal u is bounded. Denote $\rho(t) = \xi(t) - u\tanh^2(u^{\varsigma})$, where $|\rho(t)| \leq \bar{\rho}$, $\bar{\rho} > 0$ is a constant.

From (2.3), the dynamic of the strict feedback nonlinear system (2.1) can be reformulated as

$$\begin{aligned} \dot{x}_i &= c_i x_{i+1} + f_i(\bar{x}_i),\ i = 1, 2, 3, \cdots, n-1, \\ \dot{x}_n &= \kappa(u + \rho) + f_n(\bar{x}_n),\ n \geq 2, \\ y &= x_1. \end{aligned} \tag{2.6}$$

Control objective: This paper will design an output feedback adaptive NN optimal resilient ETC method for nonlinear strict-feedback system subjected to intermittent DoS attacks and input saturation, such that the following properties hold:

1) The output x_1 of the nonlinear system can track the reference signal y_r even as DoS attacks occur;

2) All the signals of the closed-loop system are SGUUB, and the corresponding cost function achieves its minimum.

3) The Zeno behavior of the ET mechanism can be excluded.

Lemma 1 ([13,36]). For $\forall(a, b) \in R^2$, the following Young's inequality can be obtained

$$ab \leq \frac{\Delta^s}{s}|a|^s + \frac{1}{h\Delta^h}|b|^h,$$

where $\Delta > 0$, $s > 1$, $h > 1$, and $(s-1)(h-1) = 1$.

Assumption 1 ([31,37]). Assume that the reference signal y_r is smooth and its time derivatives $\dot{y}_r$ and $\ddot{y}_r$ are bounded, i.e., $|y_r| < \bar{y}_r$ and $|\dot{y}_r| < \bar{\bar{y}}_r$, where $\bar{y}_r > 0$ and $\bar{\bar{y}}_r > 0$ are two constants.

2.2. ET mechanism

In order to save network bandwidth and obtain better control performance, an ET mechanism is developed with the actual ET optimal controller and triggered condition, given as:

$$\begin{aligned}
&\wp(t) = \hat{u}^*(t) - \widehat{m}\tanh(\frac{z_n\widehat{m}}{\bar{m}}),\\
&\hat{u}(t) = \wp(t_k),\ \forall \in [t_k, t_{k+1}),\\
&t_{k+1} = \inf\{t > t_k\,||\mathfrak{q}(t)| \geq \breve{m}\},\ t_1 = 0,
\end{aligned} \tag{2.7}$$

where $\mathfrak{q}(t) = \wp(t) - \hat{u}(t)$ represents the real-time measurement error caused by ET. $\hat{u}^*(t)$ is the actual optimal controller. $\bar{m} > 0$, $\widehat{m} > 0$, and $\breve{m} > \widehat{m}$ are constants. Let t_k ($k \in Z^+$) represent the instant an event is triggered. Specifically, when condition (2.7) is activated, this instant is marked as t_{k+1}, and the control signal $u(t_{k+1})$ is then applied to the system. During the interval $t \in [t_k, t_{k+1})$ between the two ET times, the control signal $\wp(t_k)$ remains invariant.

2.3. Intermittent DoS attack model

Figure 1 illustrates the block diagram of the system under intermittent DoS attacks. Noncontinuous DoS attacks are generated by the attacker owing to limited energy resources, which reflects the intermittent feature of attack activation. Motivated by [16] and [17], let $\{t_j\}_{j\in N}$ indicate the moment of the attack. $\Pi_j := [t_j, t_j + \tau_j)$ stands for the time length of the jth DoS attack, and the communication is blocked in this time period. In addition, denote the communication block time and allowed time interval as $\Phi(\tau, t) := \bigcup_{j\in N}\Pi_j \bigcap[\tau, t]$ and $\Upsilon(\tau, t){:=}[\tau, t]/\Phi\ [\tau, t]$, respectively. Thus, when the attacker launches the attack, the controller models can be represented as

$$u^{p(t)} = \begin{cases} 0,\ t \in \Phi(0, +\infty),\\ u,\ t \in \Upsilon(0, +\infty),\end{cases}$$

where $t \in \Upsilon(0, +\infty)$ and $t \in \Phi(0, +\infty)$ denote the time instant sets where the DoS attack is dormant and active. The indicator functions $p(t) = 0/1$ is defined to represent whether the system is subject to DoS attacks at time t. Next, the general assumptions about DoS attacks are given.

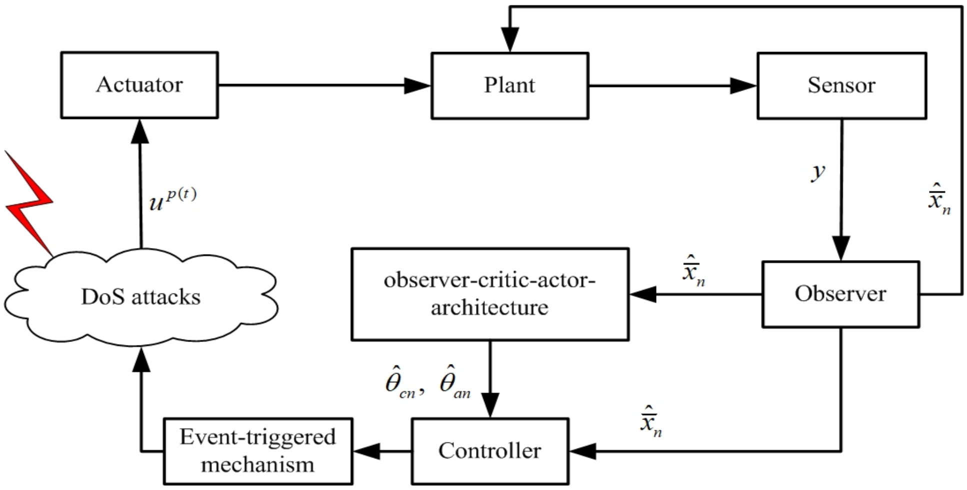

Figure 1. System block diagram under DoS attacks.

Assumption 2 (DoS Attack Frequency) ([13,16]). There exist two numbers $\ell \geq 0$ and $\tau_D > 0$ such that

$$n(\tau, t) \leq \ell + (t - \tau)/\tau_D \ ,$$

where $n(\tau, t)$ represents the attack activation number in the time interval $[\tau, t]$.
Assumption 3 (DoS Attack Duration) ([14,17]). Given a constant $T \geq 1$, such that

$$|\Phi(\tau, t)| \leq (t - \tau)/T,$$

$|\Phi(\tau, t)|$ represents the attack activated total length in the time interval $[\tau, t]$, where $\tau \leq t$ and $\tau,\ t \in R_{\geq 0}$.

2.4. NNs and function estimation

Lemma 2 ([14,20]). A continuous nonlinear function $f(x)$ is defined on a compact set Ψ. For $\forall \varepsilon_w > 0$, there exists an NN $\theta^{*T}\psi(x)$ where

$$\sup_{x\in\Psi} \left| f(x) - \theta^{*T}\psi(x) \right| < \varepsilon_w.$$

According to Lemma 2, $f(x)$ can be represented as

$$f(x) = \theta^{*T}\psi(x) + \varepsilon_w,$$

where $x \in \Psi \subset \Re^n$ is the input vector, n is a natural number, $\theta^* \in \Re^N$ stand for the weight vector with N neurons, $\varepsilon_w \leq \bar{\varepsilon}_w$ is the NN approximation error, $\bar{\varepsilon}_w$ is a positive constant, and $\psi(x) = [\psi_1(x), \cdots, \psi_i(x), \cdots, \psi_N(x)]^T$, where $\psi_i(x)$ is a basis function, usually chosen as

$$\psi_i(x) = \exp(-\frac{(x - \bar{\rho}_i)^T(x - \bar{\rho}_i)}{\varpi_i^2}),$$

where ϖ_i and $\bar{\rho}_i \in \Re^n$ represent the width and the center vector of $\psi_i(x)$.

The NN weight vector θ^* can be defined as

$$\theta^* = \arg\min_{\theta\in\Omega_\theta} [\sup_{x\in\Omega_x} |f(x) - \theta\psi(x)|],$$

where Ω_θ and Ω_x are compact sets. It is worth noting that the weight θ^* is an unknown constant vector that cannot be employed directly. Thus, we employ the vector $\hat{\theta}$ to estimate θ^*. $\tilde{\theta} = \hat{\theta} - \theta^*$ is the estimation error of the NN weight.

2.5. NN state observer design

Since the states x_i $(i \geq 2)$ of the system are unmeasurable, an NN state observer will be constructed. When the system is subject to intermittent DoS attacks, it is difficult to acquire the state information of the controlled system. At this time, the NN state observer can estimate the states of the system. Based on Lemma 2, (2.6) can be written as the following state space form:

$$\begin{aligned} \dot{X} &= A_1 X + \sum_{i=1}^{n} B_i(\theta_{f,i}^{*T}\psi_{f,i}(\bar{x}_i) + \varepsilon_{f,i}) + B_n(\kappa u + \rho), \\ y &= C^T X, \end{aligned} \tag{2.8}$$

where $A_1 = \begin{bmatrix} 0 & c_1 & & \\ 0 & & \ddots & \\ \vdots & & & c_{n-1} \\ 0 & 0 & \cdots & 0 \end{bmatrix}_{n\times n}$, $B_i = \begin{bmatrix} \underbrace{0,\ldots,0}_{i-1}, 1, 0, \ldots, 0 \end{bmatrix}_{n\times 1}^T$, $X = [x_1, x_2, \cdots, x_n]^T$, $C = [1, 0, \cdots, 0]^T$, $\theta_{f,i}^*$ are the NN optimal weight vectors, $\varepsilon_{f,i}$ are the NN minimum approximation errors, $\left|\varepsilon_{f,i}\right| \leq \varepsilon_{f,i}^*$, and $\varepsilon_{f,i}^* > 0$ are constants.

In order to estimate the states of system (2.8), an NN adaptive observer is developed with the following form:

$$\begin{aligned} \dot{\hat{X}} &= A_2\hat{X} + Ky + \sum_{i=1}^{n} B_i\hat{\theta}_{f,i}^T\psi_{f,i}(\hat{\bar{x}}_i) + B_n\kappa u, \\ \hat{y} &= C^T\hat{X}, \end{aligned} \tag{2.9}$$

where $A_2 = \begin{bmatrix} -k_1 & c_1 & & \\ -k_2 & & \ddots & \\ \vdots & & & c_{n-1} \\ -k_n & 0 & \cdots & 0 \end{bmatrix}_{n\times n}$, $K = \begin{bmatrix} k_1 \\ k_2 \\ \vdots \\ k_n \end{bmatrix}$, and $\hat{X} = [\hat{x}_1, \hat{x}_2, \cdots, \hat{x}_n]^T$. k_1, k_2, and k_3 are selected such that A_2 is a Hurwitz matrix. Accordingly, given a matrix $Q_0 = Q_0^T > 0$, there exists a matrix $P = P^T > 0$, such that

$$A_2^T P + PA_2 = -Q_0. \tag{2.10}$$

From Lemma 2, (2.8), and (2.9), the observer error dynamics can be calculated as

$$\begin{aligned}\dot{\tilde{X}} &= A_2\tilde{X} + \sum_{i=1}^{n} B_i\tilde{\theta}_{f,i}^T\psi_{f,i}(\hat{\bar{x}}_i) + \sum_{i=1}^{n} B_i\varepsilon_i^{'} - B_n\kappa\rho \\ &= A_2\tilde{X} + \sum_{i=1}^{n} B_i\tilde{\theta}_{f,i}^T\psi_{f,i}(\hat{\bar{x}}_i) + \bar{\varepsilon} - B_n\kappa\rho,\end{aligned} \tag{2.11}$$

where $\bar{\varepsilon} = [\varepsilon_1^{'}, \varepsilon_2^{'}, \cdots, \varepsilon_n^{'}]^T$ and $\varepsilon_i^{'} = {\theta_{f,i}^*}^T(\psi_{f,i}(\hat{\bar{x}}_i) - \psi_{f,i}(\bar{x}_i)) - \varepsilon_{f,i}$. $\tilde{X} = \hat{X} - X = [\tilde{x}_1, \tilde{x}_2, \cdots, \tilde{x}_n]^T$ is the estimate error by the observer. Assume there exist constants $\varepsilon_i^{'*} \geq 0$ such that $\left|\varepsilon_i^{'}\right| \leq \varepsilon_i^{'*}$. $\tilde{\theta}_{f,i} = \hat{\theta}_{f,i} - \theta_{f,i}^*$ is the NN approximate error.

Similarly, when the system suffers DoS attacks, i.e., control input $u = 0$, the NN state observer can be rewritten as

$$\begin{aligned}\dot{\hat{X}} &= A_2\hat{X} + Ky + \sum_{i=1}^{n} B_i\hat{\theta}_{f,i}^T\psi_{f,i}(\hat{\bar{x}}_i), \\ \hat{y} &= C^T\hat{X}.\end{aligned} \tag{2.12}$$

3. Adaptive NN output feedback optimized resilient ETC design

In this subsection, an event-based adaptive neural network optimal resilient control scheme will be developed under DoS attacks and unmeasurable states. The backstepping architecture and the ADP algorithm are utilized to achieve the performance function minimum for the nonlinear system (2.1) under the critic-actor NN framework. Furthermore, the stability analysis of the closed-loop system is given.

3.1. Adaptive ET optimal saturation controller design

Case I. The DoS attack is not activated.

When $t \in \Upsilon(0, +\infty)$, the backstepping recursive technique can be directly used to derive the optimal control law.

Define the coordinate changes as

$$z_i = \hat{x}_i - \lambda_i, \; i = 1, 2, 3, \cdots, n-1, \tag{3.1}$$

$$z_n = \hat{x}_n - \lambda_n - \tau_{sat}, \tag{3.2}$$

where $\lambda_1 = y_r$ is the reference signal. The variable τ_{sat} will be given later in (3.17). λ_i denotes the output of the filter. The filter is introduced to overcome the drawback of the complexity explosion in the backstepping design procedure, which is depicted as

$$\omega_j\dot{\lambda}_j = \hat{\alpha}_i - \lambda_j, \; j = 2, 3, \cdots, n, \tag{3.3}$$

where $\omega_j > 0$ is a constant and $\hat{\alpha}_i(0) = \lambda_j(0)$. The input $\hat{\alpha}_i$ of the first-order filter (3.3) is the actual optimal virtual controller of step $1 \sim (n-1)$. Define $\zeta_j = \hat{\alpha}_i - \lambda_j$ as the error variable of the filter.

According to the above definition of the coordinate changes and the first-order filter, the detailed backstepping design process of the n-step is as follows.

Step $1 \sim (n-1)$**:** Employing the NN state observer (2.9) and taking the time derivative along (3.1), yields

$$\dot{z}_i = c_i\hat{x}_{i+1} + \hat{\theta}_{f,i}^T\psi_{f,i}(\hat{\bar{x}}_i) - k_i\tilde{x}_1 - \dot{\lambda}_i,\ i = 1, 2, \cdots, n-1, \tag{3.4}$$

According to the backstepping method, regard $\hat{x}_{i+1}$ as the ideal optimal virtual control α_i^*, i.e., $\alpha_i^* = \hat{x}_{i+1}$. To design the adaptive NN optimal ET controller for the z_i-subsystem, the cost function can be defined as

$$\begin{aligned} M_i^*(z_i) &= \min_{\alpha\in\phi(\Omega_{z_i})} \int_t^\infty (q_i z_i^2(\tau) + r_i\alpha_i^2(\tau))d\tau \\ &= \int_t^\infty (q_i z_i^2(\tau) + r_i{\alpha_i^*}^2(\tau))d\tau, \end{aligned} \tag{3.5}$$

where α_i refers to the virtual control in the backstepping design. $q_i(z_i(\tau))^2 + r_i(\alpha_i^*(\tau))^2$ is the utility function. $\phi(\Omega_{z_i})$ is a compact set containing origin. $q_i > 0$ and $r_i > 0$ are two constants. According to [31] and [40], the cost function (3.5) satisfies

$$M_i^*(z_i) = \bar{\eta}_i z_i^2 + M_{ci}(z_i), \tag{3.6}$$

where $M_{ci}(z_i) = -\bar{\eta}_i z_i^2 + M_i^*(z_i)$ is a continuous scalar-value function, and $\bar{\eta}_i$ is a positive constant. By the Bellman principle, define the HJB equation associated with the optimal cost function (3.5) as follows:

$$H_i(z_i, \alpha_i^*, \frac{\partial M_i^*(z_i)}{\partial z_i}) = q_i(z_i)^2 + r_i(\alpha_i^*)^2 + \frac{\partial M_i^*(z_i)}{\partial z_i}\dot{z}_i = 0. \tag{3.7}$$

Taking the derivative on both sides of (3.7), the ideal optimal virtual control α_i^* can be derived by solving $\partial H_i/\partial\alpha_i^*$ with the form

$$\alpha_i^* = -\frac{c_i\bar{\eta}_i z_i}{r_i} - \frac{c_i}{2r_i}\frac{\partial M_{ci}(z_i)}{\partial z_i}, \tag{3.8}$$

where the term $\partial M_{ci}(z_i)/\partial z_i$ in (3.8) is an unknown continuous function of the error variable z_i. From Lemma 2, an NN can be adopted to approximate $\partial M_{ci}(z_i)/\partial z_i$ on the compact set Ω_{z_i}; one has

$$\frac{\partial M_{ci}(z_i)}{\partial z_i} = {\theta_i^*}^T\psi_i(z_i) + \varepsilon_i(z_i), \tag{3.9}$$

where $\theta_i^* \in \Re^{wi}$ represent the ideal weight vectors of the NNs, and $\psi_i(z_i) \in \Re^{wi}$ represent the basis function vectors. $\varepsilon_i(z_i) \in \Re$ represent the approximation errors satisfying $|\varepsilon_i(z_i)| \le \bar{\varepsilon}_{wi}^*$ with the positive constant $\bar{\varepsilon}_{wi}^*$. Since θ_i^* in (3.9) is unknown, the observer-critic-actor architecture is established. In this architecture, the estimation vectors $\hat{\theta}_{ci}$ and $\hat{\theta}_{ai}$ of the critic NN and the actor NN can be applied to estimate θ_i^*, i.e.,

$$\frac{\partial \hat{M}_{ci}(z_i)}{\partial z_i} = \hat{\theta}_{ci}^T\psi_i(z_i), \tag{3.10}$$

$$\hat{\alpha}_i = -\frac{c_i\bar{\eta}_i z_i}{r_i} - \frac{c_i}{2r_i}\hat{\theta}_{ai}^T\psi_i(z_i), \tag{3.11}$$

where $\partial\hat{M}_{ci}(z_i)/\partial z_i$ is the estimation of the unknown function $\partial M_{ci}(z_i)/\partial z_i$.

From (3.10) and (3.11), (3.7) can be rewritten as

$$\begin{aligned} H_i(z_i, \hat{\alpha}_i, \frac{\partial\hat{M}_i(z_i)}{\partial z_i}) =& q_i(z_i)^2 + r_i(\frac{c_i\bar{\eta}_i z_i}{r_i} + \frac{c_i}{2r_i}\hat{\theta}_{ai}^T\psi_i(z_i))^2 + \Big(2\bar{\eta}_i z_i \\ &+ \hat{\theta}_{ci}^T\psi_i(z_i)\Big)(c_i\hat{\alpha}_i + \hat{\theta}_{f,i}^T\psi_{f,i}(\hat{\bar{x}}_i) - k_i\tilde{x}_1 - \dot{\lambda}_i). \end{aligned} \tag{3.12}$$

By applying the HJB equation (3.7) and its estimation (3.12), the Hamiltonian approximation error can be denoted as

$$e_{Hi} = H_i(z_i, \hat{\alpha}_i, \frac{\partial\hat{M}_i(z_i)}{\partial z_i}) - H_i(z_i, \alpha_i^*, \frac{\partial M_i^*(z_i)}{\partial z_i}) = H_i(z_i, \hat{\alpha}_i, \frac{\partial\hat{M}_i(z_i)}{\partial z_i}).$$

Inspired by [31] and [35], we can adopt the gradient descent algorithm to minimize the objective function (3.13) such that the optimal value of the Hamiltonian approximation error is yielded as

$$E_i = \frac{1}{2(\gamma_i^T\gamma_i + 1)}e_{Hi}^2, \tag{3.13}$$

where $\gamma_i = \psi_i(z_i)(c_i\hat{\alpha}_i + \hat{\theta}_{f,i}^T\psi_{f,i}(\hat{\bar{x}}_i) - k_i\tilde{x}_1 - \dot{\lambda}_i)$. From (3.12) and (3.13), to guarantee stability of the system, the updating laws $\dot{\hat{\theta}}_{ci}$ of the critic NN weights, the updating laws $\dot{\hat{\theta}}_{ai}$ of the actor NN weights, and the observer NN updating laws $\dot{\hat{\theta}}_{f,i}$ are constructed as

$$\begin{aligned} \dot{\hat{\theta}}_{ci} =& -\beta_{ci}\frac{\partial E_i}{\partial\hat{\theta}_{ci}} = -\beta_{ci}\frac{\gamma_i}{(\gamma_i^T\gamma_i + 1)}\Big((q_i - \frac{c_i^2}{r_i}\bar{\eta}_i^2)z_i^2 + \frac{c_i^2}{4r_i}(\hat{\theta}_{ai}^T\psi_i(z_i))^2 \\ &+ \gamma_i^T\hat{\theta}_{ci} + 2\bar{\eta}_i z_i(\hat{\theta}_{f,i}^T\psi_{f,i}(\hat{\bar{x}}_i) - k_i\tilde{x}_1 - \dot{\lambda}_i)\Big), \end{aligned} \tag{3.14}$$

$$\dot{\hat{\theta}}_{ai} = \frac{c_i^2 q_i}{2r_i}\psi_i(z_i)z_i - \beta_{ai}\psi_i(z_i)\psi_i^T(z_i)\hat{\theta}_{ai} + \frac{c_i^2\beta_{ci}\psi_i(z_i)}{4r_i(\gamma_i^T\gamma_i + 1)}\psi_i^T(z_i)\hat{\theta}_{ai}\gamma_i^T\hat{\theta}_{ci}, \tag{3.15}$$

$$\dot{\hat{\theta}}_{f,i} = b_i q_i z_i\psi_{f,i}(\hat{\bar{x}}_i) - \eta_i\hat{\theta}_{f,i}, \tag{3.16}$$

where $\beta_{ai} > 0$ and $\beta_{ci} > 0$ are learning rates. $b_i > 0$, $\eta_i > 0$, and $q_i > 0$ are design constants.

Step n**:** From (3.2), the time derivative of $\dot{z}_n$ satisfies $\dot{z}_n = \dot{\hat{x}}_n - \dot{\lambda}_n - \dot{\tau}_{sat}$. As mentioned in [21], the state variable τ_{sat} is introduced to provide a bounded compensation for the control input, and the initial value of τ_{sat} equals 0. The time derivative of τ_{sat} can be further denoted as

$$\dot{\tau}_{sat} = \kappa\bar{\upsilon} - \sigma\tau_{sat}, \tag{3.17}$$

where $\bar{\upsilon} = u - \hat{u}$, and σ is a positive constant.

Remark 2. It is worth noting that an auxiliary system is also utilized in [29] to handle input saturation effects, and the main differences between the two auxiliary systems can be concluded as follows:

1) The scheme in [29] adopts fractional-power terms to attain practical finite-time stability. Our

work aims to achieve optimal resilient control for nonlinear systems under DoS attacks and event-triggered constraints.

2) We use hyperbolic tangent functions to approximate the saturation model and build auxiliary systems to compensate input deviation. The auxiliary system in [29] is fundamentally customized for finite-time adaptive laws, while ours addresses coupling among event-triggered, DoS attacks, and optimal control.

From the state observers (2.7), (2.9), and (3.17), one obtains

$$\dot{z}_n = \hat{\theta}_{f,n}^T \psi_{f,n}(\hat{\bar{x}}_n) - k_n \tilde{x}_1 - \frac{\zeta_n}{\omega_n} + \kappa \hat{u} + \sigma \tau_{sat}. \tag{3.18}$$

Similarly, the cost function of the z_n-subsystem can be defined as

$$\begin{aligned} M_n^*(z_n) &= \min_{u\in\phi(\Omega_{z_n})} \int_t^\infty (q_n z_n^2(\tau) + r_n \hat{u}^2(\tau))d\tau \\ &= \int_t^\infty (q_n z_n^2(\tau) + r_n(\hat{u}^*)^2(\tau))d\tau, \end{aligned} \tag{3.19}$$

where $\phi \in (\Omega_{z_n})$ is a compact set.

Using the same approach as step $1 \sim (n-1)$, the HJB equation is established relying on the system cost function. Since the solution of the HJB equation contains unknown nonlinear dynamics, an observer-critic-actor NN architecture is established to identify the value function. Therefore, the optimal controller is designed. During the optimized control design process, to better achieve the optimal control, the actual optimal controller $\hat{u}^*$, the corresponding the critic NN weight update law $\dot{\hat{\theta}}_{cn}$, the actor NN weight updating law $\dot{\hat{\theta}}_{an}$, and the observer NN weight updating law $\dot{\hat{\theta}}_{f,n}$ can be designed as

$$\hat{u}^* = -\frac{\kappa}{2r_n}(2\bar{\eta}_n z_n + \hat{\theta}_{an}^T \psi_n(z_n)), \tag{3.20}$$

$$\begin{aligned} \dot{\hat{\theta}}_{cn} =& -\beta_{cn}\frac{\partial E_n}{\partial \hat{\theta}_{cn}} = -\beta_{cn}\frac{\gamma_n}{(\gamma_n^T\gamma_n+1)}\Big(q_n z_n^2 - \frac{\kappa^2}{r_n}(\bar{\eta}_n z_n)^2 + \gamma_n^T\hat{\theta}_{cn} + \frac{\kappa^2}{4r_n} \\ & \times (\hat{\theta}_{an}^T\psi_n(z_n))^2 + 2\bar{\eta}_n z_n(\hat{\theta}_{f,n}^T\psi_{f,n}(\hat{\bar{x}}_n) - k_n\tilde{x}_1 - \dot{\lambda}_n + \sigma\tau_{sat})\Big), \end{aligned} \tag{3.21}$$

$$\begin{aligned} \dot{\hat{\theta}}_{an} =& \frac{\kappa^2 q_n}{2r_n}\psi_n(z_n)z_n - \beta_{an}\psi_n(z_n)\psi_n^T(z_n)\hat{\theta}_{an} \\ &+ \frac{\beta_{cn}\kappa^2}{4r_n(\gamma_n^T\gamma_n+1)}\psi_n(z_n)\psi_n^T(z_n)\hat{\theta}_{an}\gamma_n^T\hat{\theta}_{cn}, \end{aligned} \tag{3.22}$$

$$\dot{\hat{\theta}}_{f,n} = b_n q_n z_n \psi_{f,n}(\hat{\bar{x}}_n) - \eta_n \hat{\theta}_{f,n}, \tag{3.23}$$

where $\beta_{an} > 0$ and $\beta_{cn} > 0$ are learning rates, and $b_n > 0$, $\eta_n > 0$, and $q_n > 0$ are design constants.

Case II. The DoS attack is activated.

In the case of the attack $t \in \Phi(0, +\infty)$, the control input $u = 0$ results in that the traditional backstepping control method cannot be utilized directly. At this point, we construct the observer that can still acquire the estimated state to guarantee system stability. From (2.8) and (2.12), one gets

$$\begin{aligned} \dot{\hat{X}} &= A_2\hat{X} + \sum_{i=1}^n B_i\hat{\theta}_{f,i}^T\psi_{f,i}(\hat{\bar{x}}_i) \\ &= A_2\hat{X} + \psi_f\hat{\theta}_f, \end{aligned} \tag{3.24}$$

where $\hat{\theta}_f^T = [\hat{\theta}_{f,1}, \cdots, \hat{\theta}_{f,n}]$, $\psi_f = diag[\psi_{f,1}, \cdots, \psi_{f,n}]$. The Lyapunov function is considered as

$$V_i = \frac{1}{2}\hat{X}^T P \hat{X} + \frac{1}{2b_i}\hat{\theta}_f^T \hat{\theta}_f. \tag{3.25}$$

The time derivative of V_i is $\dot{V}_i = 1/2\ (\dot{\hat{X}}^T P \hat{X} + \hat{X}^T P \dot{\hat{X}}) + \frac{1}{b_i}\hat{\theta}_f^T \dot{\hat{\theta}}_f$. Combining (2.10) and (3.24), one has

$$\dot{V}_i = \frac{1}{2}\hat{X}^T (A_2^T P + P A_2)\hat{X} + \hat{X}^T P \psi_f \hat{\theta}_f + \frac{1}{b_i}\hat{\theta}_f^T \dot{\hat{\theta}}_f. \tag{3.26}$$

Substituting the update law $\dot{\hat{\theta}}_f = -b_i \psi_f P \hat{X} - \eta_i \hat{\theta}_f$ into (3.26), one has

$$\begin{aligned} \dot{V}_i &= \frac{1}{2}\hat{X}^T (A_2^T P + P A_2)\hat{X} + \hat{X}^T P \psi_f \hat{\theta}_f - \hat{\theta}_f^T \psi_f P \hat{X} - \frac{\eta_i}{b_i}\hat{\theta}_f^T \hat{\theta}_f \\ &= -\frac{1}{2}\hat{X}^T Q_0 \hat{X} - \frac{\eta_i}{b_i}\hat{\theta}_f^T \hat{\theta}_f. \end{aligned} \tag{3.27}$$

From (3.27), $\dot{V}_i$ can eventually be written as

$$\dot{V}_i \le -\frac{1}{2}\hat{X}^T \lambda_{\min}(Q_0)\hat{X} - \frac{\eta_i}{b_i}\hat{\theta}_i^T \hat{\theta}_i. \tag{3.28}$$

where $\lambda_{\min}(Q_0)$ is the smallest eigenvalue of matrix Q_0. According to (3.28) and [14], when the DoS attack is activated, i.e., $u = 0$, it is concluded that the stability of the state observer can be guaranteed.

3.2. Stability analysis

The stability analysis of the adaptive NN optimal resilient ETC control method can be concluded by the following theorem.

Theorem 1. For the strict feedback uncertain nonlinear system (2.1), the ET mechanism (2.7), the NN state observer (2.9), the optimal virtual controls (3.11) and (3.20), the critic NN updating laws (3.14) and (3.21), the actor NN updating laws (3.15) and (3.22), and the observer NN updating laws (3.16) and (3.23) are designed. The overall control method can achieve the following:

1) The signals $z_n, \tilde{\theta}_{cn}, \tilde{\theta}_{an}, \tilde{\theta}_{f,n}, \tilde{X}, \zeta_j\ (j = 2, 3, \cdots, n)$, and τ_{sat} of the closed-loop system are SGUUB.

2) Tracking error $x_1 - y_r$ converges to a small neighborhood containing the origin.

Remark 3. It is worth emphasizing that the established stability results of closed-loop system are SGUUB. This is because NNs are utilized to approximate unknown nonlinear functions, and the universal approximation property holds over a predefined compact set. Within this compact set, by selecting sufficiently large control gains and appropriate adaptive parameters, the tracking error and all signals in the closed-loop system can be guaranteed to be SGUUB. Since the compact set can be chosen arbitrarily large to cover the system's desired operating range, the system signals are guaranteed to be SGUUB.

Proof. Consider the total Lyapunov function candidate as

$$V = V_0 + \cdots + V_i + \cdots + V_n,\ i \le 1, 2, \cdots, n-1, \tag{3.29}$$

where

$$\begin{aligned}V_0 &= \frac{1}{2}\tilde{X}^T P\tilde{X},\\ V_i &= \frac{q_i}{2}z_i^2 + \frac{1}{2}\tilde{\theta}_{ci}^T\tilde{\theta}_{ci} + \frac{1}{2}\tilde{\theta}_{ai}^T\tilde{\theta}_{ai} + \frac{1}{2b_i}\tilde{\theta}_{f,i}^T\tilde{\theta}_{f,i} + \frac{1}{2}\zeta_{i+1}^2,\\ V_n &= \frac{q_n}{2}z_n^2 + \frac{1}{2}\tilde{\theta}_{cn}^T\tilde{\theta}_{cn} + \frac{1}{2}\tilde{\theta}_{an}^T\tilde{\theta}_{an} + \frac{1}{2b_n}\tilde{\theta}_{f,n}^T\tilde{\theta}_{f,n} + \frac{1}{2}\tau_{sat}^2.\end{aligned}$$

$\tilde{\theta}_{an} = \hat{\theta}_{an} - \theta_n^*$, $\tilde{\theta}_{cn} = \hat{\theta}_{cn} - \theta_n^*$, and $\tilde{\theta}_{f,n} = \hat{\theta}_{f,n} - \theta_{f,n}^*$ are the approximate error of the actor NN, critic NN, and the observer NN, respectively.

The time derivative of V_0 is $\dot{V}_0 = 1/2\ (\dot{\tilde{X}}^T P\tilde{X} + \tilde{X}^T P\dot{\tilde{X}})$. According to (2.10) and (2.11), one has

$$\begin{aligned}\dot{V}_0 =& -\frac{1}{2}\tilde{X}^T Q_0\tilde{X} + \tilde{X}^T P\sum_{i=1}^{n} B_i(\tilde{\theta}_{f,i}^T\psi_{f,i}(\hat{\tilde{x}}_i) + \varepsilon_i^{'}) - \tilde{X}^T PB_n\kappa\rho\\ \leq& -\frac{1}{2}\lambda_{\min}(Q_0)\left\|\tilde{X}\right\|^2 + \tilde{X}^T P(\sum_{i=1}^{n} B_i\tilde{\theta}_{f,i}^T\psi_{f,i}(\hat{\tilde{x}}_i) + \bar{\varepsilon} - B_n\kappa\rho).\end{aligned} \tag{3.30}$$

where $\bar{\varepsilon}$ is defined in (2.11), and $\bar{\varepsilon} < \bar{\varepsilon}^*$ with $\bar{\varepsilon}^* > 0$. According to Lemma 1 and the fact $\psi_{f,i}^T(\hat{\tilde{x}}_i)\psi_{f,i}(\hat{\tilde{x}}_i) \leq \mathfrak{P}$, one gets

$$\begin{aligned}&\tilde{X}^T P\sum_{i=1}^{n} B_i\tilde{\theta}_{f,i}^T\psi_{f,i}(\hat{\tilde{x}}_i) + \tilde{X}^T P\bar{\varepsilon} - \tilde{X}^T PB_n\kappa\rho\\ \leq&\frac{3}{2}\left\|\tilde{X}\right\|^2 + \frac{1}{2}\|P\|^2(\mathfrak{P}\left\|\tilde{\theta}_f\right\|^2 + \|\bar{\varepsilon}^*\|^2 + (\kappa\rho)^2),\end{aligned} \tag{3.31}$$

where $\tilde{\theta}_f = [\tilde{\theta}_{f,1}, \cdots, \tilde{\theta}_{f,n}]^T$, and $\mathfrak{P} > 0$ is a constant. From (3.31), $\dot{V}_0$ can be re-expressed as

$$\dot{V}_0 \leq -(\frac{1}{2}\lambda_{\min}(Q_0) - \frac{3}{2})\left\|\tilde{X}\right\|^2 + \frac{1}{2}\|P\|^2\mathfrak{P}\left\|\tilde{\theta}_f\right\|^2 + d_0, \tag{3.32}$$

where $d_0 = \frac{1}{2}\|P\|^2(\|\bar{\varepsilon}^*\|^2 + (\kappa\rho)^2)$.

From (3.8) and (3.9), the HJB equation (3.7) can be rewritten as

$$\begin{aligned}H_i(z_i, \alpha_i^*, \frac{\partial M_i^*(z_i)}{\partial z_i}) =& -\frac{c_i^2}{r_i}(\bar{\eta}_i z_i)^2 + q_i z_i^2 - \frac{c_i^2\bar{\eta}_i z_i}{r_i}\theta_i^{*T}\psi_i(z_i)\\ &+ (2\bar{\eta}_i z_i + \theta_i^{*T}\psi_i(z_i))(\hat{\theta}_{f,i}^T\psi_{f,i}(\hat{\tilde{x}}_i) - k_i\tilde{x}_1 - \dot{\lambda}_i)\\ &- \frac{c_i^2}{4r_i}(\theta_i^{*T}\psi_i(z_i))^2 + \bar{\varepsilon}_{Hi} = 0,\end{aligned} \tag{3.33}$$

where $\bar{\varepsilon}_{Hi} = \varepsilon_i(z_i)(c_i\alpha_i^* + \hat{\theta}_{f,i}^T\psi_{f,i}(\hat{\tilde{x}}_i) - k_i\tilde{x}_1 - \dot{\lambda}_i) + \frac{c_i^2}{4r_i}\varepsilon_i^2(z_i)$ is bounded. Adding and subtracting $\gamma_i^T\theta_i^*$ on the right side of (3.33), one has

$$\begin{aligned}q_i z_i^2 - \frac{c_i^2}{r_i}(\bar{\eta}_i z_i)^2 =& -\gamma_i^T\theta_i^* - \frac{c_i^2}{2r_i}\theta_i^{*T}\psi_i(z_i)\hat{\theta}_{ai}^T\psi_i(z_i) + \frac{c_i^2}{4r_i}\theta_i^{*T}\psi_i(z_i)\\ &\times\psi_i^T(z_i)\theta_i^* - 2\bar{\eta}_i z_i(\hat{\theta}_{f,i}^T\psi_{f,i}(\hat{\tilde{x}}_i) - k_i\tilde{x}_1 - \dot{\lambda}_i) - \bar{\varepsilon}_{Hi}.\end{aligned} \tag{3.34}$$

According to the filter (3.3), the time derivative of the filter error λ_{i+1} is given by

$$\dot{\lambda}_{i+1} = B_{i+1}(z_i, \hat{\theta}_{ai}) - \frac{\zeta_{i+1}}{\omega_{i+1}}, \ i = 1, 2, \cdots n-1, \tag{3.35}$$

where $B_i(z_i, \hat{\theta}_{ai}) = -\frac{c_i \bar{\eta}_i}{r_i}\dot{z}_i - \frac{c_i}{2r_i}\dot{\hat{\theta}}_{ai}^T \psi_i(z_i) - \frac{c_i}{2r_i}\hat{\theta}_{ai}^T \dot{\psi}_i(z_i)\dot{z}_i$. Motivated by [21], for any $p_0 > 0$, the sets Ω_j are defined as

$$\left[\sum_{i=1}^{j}(z_i^2 + \frac{1}{b_i}\tilde{\theta}_{f,i}^T \tilde{\theta}_{f,i}) + \sum_{i=1}^{j}\zeta_{i+1}^2 \le 2p_0\right] \in R^{\sum_{i=1}^{j} n_i + 2j - 1}, \tag{3.36}$$

where $j = 1, 2, \cdots, n$, $\zeta_{n+1} = 0$, n_i are the dimensionality of the NN estimation error $\tilde{\theta}_{f,i}$, the sets Ω_j are compact, and $\left|B_{i+1}(z_i, \hat{\theta}_{ai})\right|$ has an upper bound $\bar{B}_{i+1}$ on Ω_j, i.e., $\left|B_{i+1}(z_i, \hat{\theta}_{ai})\right| \le \bar{B}_{i+1}$, and satisfies $\bar{B}_{i+1} > 0$ is a constant.

From (3.3), (3.4), (3.11), and $z_n = \hat{x}_n - \lambda_n - \tau_{sat}$, $\dot{z}_i$ $(i = 1, 2, \cdots, n-1)$ can be reformulated as

$$\begin{aligned}\dot{z}_i =& c_i\Big(z_{i+1} - \frac{c_i \bar{\eta}_i z_i}{r_i} - \frac{c_i}{2r_i}\hat{\theta}_{ai}^T \psi_i(z_i) - \zeta_{i+1} \\ &+ \nu_0(i)\tau_{sat}\Big) + \hat{\theta}_{f,i}^T \psi_{f,i}(\hat{\bar{x}}_i) - k_i \tilde{x}_1 - \dot{\lambda}_i,\end{aligned} \tag{3.37}$$

where the function $\nu_0(i) = 1$ if $i = n-1$, else $\nu_0(i) = 0$. The time derivative of V_i along Eqs (3.14)–(3.16), (3.34), (3.35), and (3.37) is

$$\begin{aligned}\dot{V}_i =& q_i z_i\Big(c_i\Big(z_{i+1} - \frac{c_i \bar{\eta}_i z_i}{r_i} - \frac{c_i}{2r_i}\hat{\theta}_{ai}^T \psi_i(z_i) - \zeta_{i+1} \\ &+ \nu_0(i)\tau_{sat}\Big) + \hat{\theta}_{f,i}^T \psi_{f,i}(\hat{\bar{x}}_i) - k_i \tilde{x}_1 - \dot{\lambda}_i\Big) \\ &- \beta_{ci}\frac{\tilde{\theta}_{ci}^T \gamma_i}{(\gamma_i^T \gamma_i + 1)}\Big(\gamma_i^T \tilde{\theta}_{ci} - \frac{c_i^2}{2r_i}\theta_i^{*T}\psi_i(z_i)\hat{\theta}_{ai}^T \psi_i(z_i) \\ &+ \frac{c_i^2}{4r_i}\theta_i^{*T}\psi_i(z_i)\psi_i^T(z_i)\theta_i^* - \bar{\varepsilon}_{Hi} + \frac{c_i^2}{4r_i}(\hat{\theta}_{ai}^T \psi_i(z_i))^2\Big) \\ &+ \tilde{\theta}_{ai}^T\Big(\frac{c_i^2 q_i}{2r_i}\psi_i(z_i)z_i - \beta_{ai}\psi_i(z_i)\psi_i^T(z_i)\hat{\theta}_{ai} \\ &+ \frac{c_i^2 \beta_{ci}}{4r_i(\gamma_i^T \gamma_i + 1)}\psi_i(z_i)\psi_i^T(z_i)\hat{\theta}_{ai}\gamma_i^T \hat{\theta}_{ci}\Big) \\ &+ \frac{1}{b_i}\tilde{\theta}_{f,i}^T(b_i q_i z_i \psi_{f,i}(\hat{\bar{x}}_i) - \eta_i \hat{\theta}_{f,i}) + \zeta_{i+1}(-\frac{\zeta_{i+1}}{\omega_{i+1}} + B_{i+1}).\end{aligned} \tag{3.38}$$

By using the fact

$$\begin{aligned}\beta_{ai}\tilde{\theta}_{ai}^T \psi_i(z_i)\psi_i^T(z_i)\hat{\theta}_{ai} =& \frac{\beta_{ai}}{2}\tilde{\theta}_{ai}^T \psi_i(z_i)\psi_i^T(z_i)\tilde{\theta}_{ai} + \frac{\beta_{ai}}{2}\hat{\theta}_{ai}^T \psi_i(z_i) \\ &\times \psi_i^T(z_i)\hat{\theta}_{ai} - \frac{\beta_{ai}}{2}\theta_i^{*T}\psi_i(z_i)\psi_i^T(z_i)\theta_i^*,\end{aligned} \tag{3.39}$$

$$
\begin{aligned}
&-\frac{c_i^2}{2r_1}\theta_i^{*T}\psi_i(z_i)\hat{\theta}_{ai}^T\psi_i(z_i)+\frac{c_i^2}{4r_i}\theta_i^{*T}\psi_i(z_i)\\
&\times\psi_i^T(z_i)\theta_i^*+\frac{c_i^2}{4r_i}\hat{\theta}_{ai}^T\psi_i(z_i)\psi_i^T(z_i)\hat{\theta}_{ai}\\
=&\frac{c_i^2}{4r_i}\hat{\theta}_{ai}^T\psi_i(z_i)\psi_i^T(z_i)\tilde{\theta}_{ai}-\frac{c_i^2}{4r_i}\tilde{\theta}_{ai}^T\psi_i(z_i)\psi_i^T(z_i)\theta_i^*,
\end{aligned}
\tag{3.40}
$$

and Lemma 1, together with the assumption that $\theta_i^{*T}\psi_i(z_i)\psi_i^T(z_i)\theta_i^*\le\pi_i$, where $\pi_i>0$. $\dot{V}_i$ can be finally written as

$$
\begin{aligned}
\dot{V}_i\le&-q_i\bar{q}_iz_i^2-(\frac{\eta_i}{2b_i}-q_i)\tilde{\theta}_{f,i}^T\tilde{\theta}_{f,i}+\widehat{\omega}_i+\frac{q_ik_i^2}{2}\left\|\tilde{X}\right\|^2+d_i+\frac{q_ic_i}{2}z_{i+1}^2\\
&-(\beta_{ci}\frac{1}{2(\gamma_i^T\gamma_i+1)}-\frac{c_i^2}{8r_i}\frac{\pi_i}{(\gamma_i^T\gamma_i+1)})\tilde{\theta}_{ci}^T\gamma_i{\gamma_i}^T\tilde{\theta}_{ci}\\
&-(\frac{\beta_{ai}}{2}-\frac{c_i^2}{8r_i(\gamma_i^T\gamma_i+1)})\hat{\theta}_{ai}^T\psi_i(z_i)\psi_i^T(z_i)\hat{\theta}_{ai}+\frac{q_ic_i}{2}\upsilon_0(i)(\tau_{sat})^2\\
&-(\frac{\beta_{ai}}{2}-\frac{c_i^2\beta_{ci}^2(1+\theta_i^{*T}\gamma_i\gamma_i^T\theta_i^*)}{8r_i(\gamma_i^T\gamma_i+1)})\tilde{\theta}_{ai}^T\psi_i(z_i)\psi_i^T(z_i)\tilde{\theta}_{ai},
\end{aligned}
\tag{3.41}
$$

where $\widehat{q}_1=\frac{(4\bar{\eta}_1-1)c_1^2-4r_1c_1-10r_1}{4r_1}$, $\bar{q}_i=\frac{(4\bar{\eta}_i-1)c_i^2-4r_ic_i-2r_ic_i\nu_0(i)-10r_i}{4r_i}$, $\widehat{\omega}_1=-(\frac{1}{\omega_2}-\frac{q_1c_1}{2}-\frac{1}{2})$, $d_1=\frac{\beta_{c1}}{2(\gamma_1^T\gamma_1+1)}\bar{\varepsilon}_1^2+\frac{c_1^2q_1}{4r_1}\theta_1^{*T}\theta_1^*+(\frac{q_1}{2}+\frac{\eta_1}{2b_1})\theta_{f,1}^{*T}\theta_{f,1}^*+\frac{q_1}{2}\bar{\dot{y}}_r^2+\frac{1}{2}\bar{B}_2^2$, $\widehat{\omega}_i=-(\frac{1}{\omega_{i+1}}-\frac{1}{2}-\frac{q_ic_i}{2})+\frac{q_i}{2\omega_i^2}$ $(i=2,3,\cdots,n-1)$, and $d_i=\frac{\beta_{ci}}{2(\gamma_i^T\gamma_i+1)}\bar{\varepsilon}_{Hi}^2+\frac{c_i^2q_i}{4r_i}\theta_i^{*T}\theta_i^*++\frac{q_i}{2}\theta_{f,i}^{*T}\theta_{f,i}^*+\frac{\eta_i}{2b_i}\theta_{f,i}^{*T}\theta_{f,i}^*+\frac{1}{2}\bar{B}_{i+1}^2$ $(i=2,3,\cdots,n-1)$.

During the time interval $t\in[t_k,t_{k+1})$, we have $|\wp(t)-\hat{u}(t)|\le\breve{m}$. Therefore, there exists a time-varying parameter $\bar{\lambda}(t)$ such that $\bar{\lambda}(t_k)=0$, $\bar{\lambda}(t_{k+1})=\pm1$, $|\bar{\lambda}(t)|\le1$ for all $t\in[t_k,t_{k+1})$, and $\wp(t)=\hat{u}(t)+\bar{\lambda}(t)\breve{m}$. From (2.7), (3.18), and (3.20), $\dot{z}_n$ can be rewritten as

$$
\begin{aligned}
\dot{z}_n=&\hat{\theta}_{f,n}^T\psi_{f,n}(\hat{\bar{x}}_n)-k_n\tilde{x}_1-\frac{\zeta_n}{\omega_n}-\frac{\kappa^2}{2r_n}(2\bar{\eta}_nz_n+\hat{\theta}_{an}^T\psi_n(z_n))\\
&-\kappa\widehat{m}\tanh(\frac{z_n\widehat{m}}{\bar{m}})-\kappa\bar{\lambda}(t)\breve{m}+\sigma\tau_{sat}.
\end{aligned}
\tag{3.42}
$$

The time derivative of the Lyapunov function V_n is

$$
\dot{V}_n=q_nz_n\dot{z}_n+\tilde{\theta}_{cn}^T\dot{\tilde{\theta}}_{cn}+\tilde{\theta}_{an}^T\dot{\tilde{\theta}}_{an}+\frac{1}{b_n}\tilde{\theta}_{f,n}^T\dot{\tilde{\theta}}_{f,n}+\tau_{sat}\dot{\tau}_{sat}.
\tag{3.43}
$$

According to [32], we have $|\bar{g}|-\bar{g}\tanh(\bar{g}/\widehat{g}\ )\le\bar{\kappa}\widehat{g}$, where $\bar{\kappa}=0.2785$, $\widehat{g}\in R^+$, and $\bar{g}\in R$.

Substituting (3.17), (3.21)–(3.23), and (3.42) into (3.43), we can get

$$
\begin{aligned}
\dot{V}_n \leq & - q_n\bar{q}_n z_n^2 - (\frac{\eta_n}{2b_n} - q_n)\tilde{\theta}_{f,n}^T\tilde{\theta}_{f,n} + \frac{q_n k_n^2}{2}\left\|\tilde{X}\right\|^2 \\
& - (\beta_{cn}\frac{1}{2(\gamma_n^T\gamma_n+1)} - \frac{c_n^2}{8r_n}\frac{\pi_n}{(\gamma_n^T\gamma_n+1)})\tilde{\theta}_{cn}^T\gamma_n{\gamma_n}^T\tilde{\theta}_{cn} \\
& - (\frac{\beta_{an}}{2} - \frac{c_n^2}{8r_n(\gamma_n^T\gamma_n+1)})\hat{\theta}_{an}^T\psi_n(z_n)\psi_n^T(z_n)\hat{\theta}_{an} \\
& - (\frac{\beta_{an}}{2} - \frac{c_n^2\beta_{cn}^2(1+\theta_n^{*T}\gamma_n\gamma_n^T\theta_n^*)}{8r_n(\gamma_n^T\gamma_n+1)})\tilde{\theta}_{an}^T\psi_n(z_n)\psi_n^T(z_n)\tilde{\theta}_{an} \\
& - (\sigma - \frac{\kappa}{2} - \frac{q_n}{2}\sigma^2)\tau_{sat}^2 + \widehat{\omega}_n + d_n,
\end{aligned}
\tag{3.44}
$$

where $\bar{q}_n = \frac{(4\bar{\eta}_n-1)c_n^2-12r_n}{4r_n} - \frac{1}{2}$, $\widehat{\omega}_n = \frac{q_n}{2\omega_n^2}$, and $d_n = \frac{\beta_{cn}}{2(\gamma_n^T\gamma_n+1)}\bar{\varepsilon}_{Hn}^2 + \frac{\kappa^2 q_n}{4r_n}\theta_n^{*T}\theta_n^* + (\frac{q_n}{2} + \frac{\eta_n}{2b_n})\theta_{f,n}^{*T}\theta_{f,n}^* + \frac{\kappa}{2}\bar{\upsilon}^2 + \frac{1}{2}q_n\bar{\kappa}^2\kappa^2\bar{m}^2$. Combining (3.32), (3.41), and (3.44), $\dot{V}$ can be written as

$$
\begin{aligned}
\dot{V} \leq & - \widehat{\lambda}\left\|\tilde{X}\right\|^2 - \sum_{i=1}^{n}\widehat{q}_i q_i z_i^2 - \sum_{l=1}^{n}\varpi_{cl}\tilde{\theta}_{cl}^T\tilde{\theta}_{cl} - \sum_{l=1}^{n}\varpi_{al}\tilde{\theta}_{al}^T\tilde{\theta}_{al} \\
& - \sum_{l=1}^{n}\varpi_{all}\hat{\theta}_{al}^T\hat{\theta}_{al} - \widehat{b}\tilde{\theta}_{f,l}^T\tilde{\theta}_{f,l} - \sum_{l=1}^{n}\widehat{\omega}_l\zeta_{l+1}^2 - \widehat{\tau}\tau_{sat}^2 + d,
\end{aligned}
\tag{3.45}
$$

where $\widehat{\lambda} = \frac{1}{2}\lambda_{\min}(Q_0) - \frac{3}{2} - \sum_{i=1}^{n}\frac{q_i k_i^2}{2}$, $\widehat{\omega}_l = (\frac{1}{\omega_{l+1}} - \frac{1}{2} - \frac{q_l c_l}{2} + \frac{q_l}{2\omega_{l+1}^2})$, $\widehat{q}_i = \bar{q}_i - \frac{q_{i-1}c_{i-1}}{2}$ $(2 \leq i \leq n)$,$\widehat{b} = \sum_{l=1}^{n}(\frac{\eta_l}{2b_l} - q_l) - \frac{1}{2}\|P\|^2\mathfrak{P}$, $\widehat{\tau} = (\sigma - \frac{\kappa}{2} - \frac{q_n}{2}\sigma^2 - \frac{q_{n-1}c_{n-1}}{2})$,$\varpi_{cl} = (\frac{\beta_{cl}}{2} - \frac{c_l^2\pi_l}{8r_l})\frac{\gamma_l^T\gamma_l}{(\gamma_l^T\gamma_l+1)}$,$\varpi_{al} = (\frac{\beta_{al}}{2} - \frac{c_l^2\beta_{al}^2(1+\theta_l^{*T}\gamma_l\gamma_l^T\theta_l^*)}{8r_l(\gamma_l^T\gamma_l+1)})\pi_{\psi_l}$, $\varpi_{all} = (\frac{\beta_{al}}{2} - \frac{c_l^2}{8r_l(\gamma_l^T\gamma_l+1)})\pi_{\psi_l}$, $\left\|\psi_l(z_l)\psi_l^T(z_l)\right\| \leq \pi_{\psi_l}$, $d = d_0 + \sum_{l=1}^{n}d_l$, and $d = \sup_{t\geq 0}\{d(t)\}$.

Let

$$
\begin{aligned}
\varphi = \min_{i=1,2,\cdots,n} & \{2\widehat{\lambda}, 2\widehat{q}_1, \cdots, 2\widehat{q}_n, 2\varpi_{a1}, \cdots, 2\varpi_{an}, 2\varpi_{c1}, \\
& \cdots, 2\varpi_{cn}, 2\varpi_{a11}, \cdots, 2\varpi_{ann}, 2\widehat{b}, 2\widehat{\omega}_i, 2\widehat{\tau}\}.
\end{aligned}
\tag{3.46}
$$

Thus, (3.45) can be reformulated as

$$
\dot{V}(t) \leq -\varphi V(t) + d. \tag{3.47}
$$

It is obvious to known that $W(t) = e^{\varphi t}V^{p(t)}(X(t))$ is piecewise differentiable along the solution of the strict feedback nonlinear system (2.1) with DoS attacks. In view of (3.47), at each interval $[t_j, t_{j+1}]$ of DoS attacks, one obtains

$$
\begin{aligned}
\dot{W}(t) = & \varphi e^{\varphi t}V^{p(t)}(X(t)) + e^{\varphi t}\dot{V}^{p(t)}(X(t)) \\
\leq & d e^{\varphi t}, \ t \in [t_j, t_{j+1}].
\end{aligned}
\tag{3.48}
$$

Combining (3.48) with $V_k(X(t)) \le \mu V_l(X(t)),\ \forall k, l \in N$, one has

$$\begin{aligned} W(t_{j+1}) =& e^{\varphi t_{j+1}} V^{p(t_{j+1})}(X(t_{j+1})) \\ \le& \mu e^{\varphi t_{j+1}} V^{p(t_j)}(X(t_{j+1})) = \mu W(t_{j+1}^-) \\ \le& \mu \left[W(t_j) + \int_{t_j}^{t_{j+1}} d e^{\varphi t} dt \right], \end{aligned} \tag{3.49}$$

where $\mu = \max\left[\lambda_{\max}(P)/\lambda_{\min}(P)\right]$, and satisfies $\mu \ge 1$. Selecting an arbitrary $\tau > t_0 = 0$, (3.49) can be integrated from $j = 0$ to $j = n(0,\tau) - 1$, and one gets

$$\begin{aligned} W(\tau^-) \le& W(t_{n(0,\tau)}) + \int_{t_{n(0,\tau)}}^{\tau} d e^{\varphi t} dt \\ \le& \mu \left[W(t_{n(0,\tau)-1}) + \int_{t_{n(0,\tau)-1}}^{t_{n(0,\tau)}} d e^{\varphi t} dt + \mu^{-1} \int_{t_{n(0,\tau)}}^{\tau} d e^{\varphi t} dt \right] \le \cdots \\ \le& \mu^{n(0,\tau)} \left[W(0) + \sum_{j=0}^{n(0,\tau)-1} \mu^{-j} \int_{t_j}^{t_{j+1}} d e^{\varphi t} dt + \mu^{-n(0,\tau)} \int_{t_{n(0,\tau)}}^{\tau} d e^{\varphi t} dt \right]. \end{aligned} \tag{3.50}$$

Since $\tau_D > (\ln\mu/\varphi)$, for any $\delta \in (0, \varphi - \ln\mu/\tau_D)$, based on Assumption 2, one gets

$$n(\tau, t) \le \ell + \frac{(\varphi - \delta)(t - \tau)}{\ln\mu},\ \forall \mathrm{t} \ge \tau \ge 0. \tag{3.51}$$

In addition, since $n(0,\tau) - j \le 1 + n(\tau, t_{j+1}),\ j = 0, 1, \cdots, n(0,\tau)$. Thus,

$$\mu^{n(0,\tau)-j} \le \mu^{1+\ell} e^{(\varphi-\delta)(\tau - t_{j+1})}. \tag{3.52}$$

Furthermore, noting $\delta < \varphi$, one obtains

$$\int_{t_j}^{t_{j+1}} d e^{\varphi t} dt \le e^{(\varphi-\delta) t_{j+1}} \int_{t_j}^{t_{j+1}} d e^{\delta t} dt. \tag{3.53}$$

It then follows from (3.52) and (3.53) that

$$W(\tau^-) \le \mu^{n(0,\tau)} W(0) + \mu^{1+\ell} e^{(\varphi-\delta)\tau} \int_0^{\tau} d e^{\delta t} dt, \tag{3.54}$$

which indicates that

$$\begin{aligned} \bar{\alpha}(\|X(\tau)\|) \le& V^{p(\tau^-)}(X(\tau^-)) \\ \le& e^{\ell \ln\mu} e^{(\frac{\ln\mu}{\tau_D} - \varphi)\tau} \alpha(\|X(0)\|) + \mu^{1+\ell \frac{d}{\delta}} (1 - e^{-\delta\tau}) \\ \le& e^{\ell \ln\mu} e^{(\frac{\log\mu}{\tau_D} - \varphi)\tau} \alpha(\|X(0)\|) + \mu^{1+\ell \frac{d}{\delta}},\ \forall\ \delta > 0,\ \tau > 0. \end{aligned} \tag{3.55}$$

Invoking (3.55), it is proven that the researched observer-based NN optimal resilient control scheme can guarantee that all signals z_i $(i = 1, 2, \cdots, n)$, $\tilde{X}$, ζ_{i+1} (ζ_{n+1}=0), τ_{sat}, $\tilde{\theta}_{f,i}$, $\tilde{\theta}_{ci}$, and $\tilde{\theta}_{ai}$ are SGUUB.

We now prove that there always exists a time interval $t^* > 0$ such that $t_{k+1} - t_k \ge t^*$ for all $k \in Z^+$ between any two consecutive triggering events. From $\mathfrak{q}(t) = \wp(t) - \hat{u}(t),\ \forall t \in [t_k, t_{k+1})$, we have

$\frac{d}{dt}|\mathfrak{q}(t)| = \frac{d}{dt}(\mathfrak{q}(t) * \mathfrak{q}(t))^{\frac{1}{2}} = \mathrm{sign}(\mathfrak{q}(t))\dot{\mathfrak{q}}(t) \le |\dot{\wp}(t)|$. According to (2.7), we have $\dot{\wp}(t) = \dot{\hat{u}}^*(t) - \frac{\widehat{m}\dot{z}_n}{\cosh^2(z_n\widehat{m}/\bar{m})}$. Given the aforementioned analysis, we recognize that all signals are bounded. Therefore, we can derive that there must exists constant $\bar{\mathfrak{q}}^* > 0$ such that $|\dot{\wp}(t)| \le \bar{\mathfrak{q}}^*$ holds. Noting that $\mathfrak{q}(t_k) = 0$ and $\lim_{t\to t_{k+1}} \mathfrak{q}(t) = \breve{m}$, it follows that there must exists a positive constant t^* satisfying $t^* \ge \breve{m}/\bar{\mathfrak{q}}^*$, which implies that the Zeno behavior of the proposed ETC mehcanism can be excluded. ■

Remark 4. In order to illustrate the principles for parameter selection, the parameter selection guidelines for the presented optimal resilient event-triggered control algorithm can be described as follows:

1) The design parameters $\bar{m}$, $\widehat{m}$, $\breve{m}$, and $\breve{m} > \widehat{m}$ are chosen to determine the event-triggered mechanism;

2) The parameters T, τ_D, and ℓ of the DoS attack model are chosen to determine the frequency of DoS attack;

3) The observer gains k_i in (2.9) are chosen such that A_2 is a Hurwitz matrix;

4) The design parameters r_i and $\bar{\eta}_i$ in (3.11) and (3.20) are chosen as $r_i > 0$ and $\bar{\eta}_i > 0$;

5) The design parameters $\beta_{ai}, \beta_{ci}, b_i, \eta_i$, and q_i are chosen to determine the update laws (3.14)–(3.16) and (3.21)–(3.23). The simulation section shows the specified parameters.

4. Simulation study

In this section, we provide numerous practical simulation examples to verify the effectiveness of the presented optimal resilient control algorithm.

Consider the single-phase grid-connected PV power system [19, 23] illustrated in Figure 2, which is composed of a PV array, a full-bridge inverter circuit, and an LCL filter circuit. In the circuit model, Q_1, Q_2, Q_3, and Q_4 represent the MOS transistors, L_1 and L_2 indicate inductors, and C_1 and C_2 are capacitors. The LCL filter circuit connects with the power grid, and it is composed of L_1, C_1, and L_2. R_1 and R_2 are the equivalent resistances of L_1 and L_2. There are identical duty cycles for Q_1 and Q_4, as well as for Q_2 and Q_3. Based on the properties of the full-bridge inverter circuit in the PV power generation system, when $u > 0$, Q_1 and Q_4 are opened, and Q_2 and Q_3 are closed. The direction of the current flow is counterclockwise. On the contrary, it is clockwise.

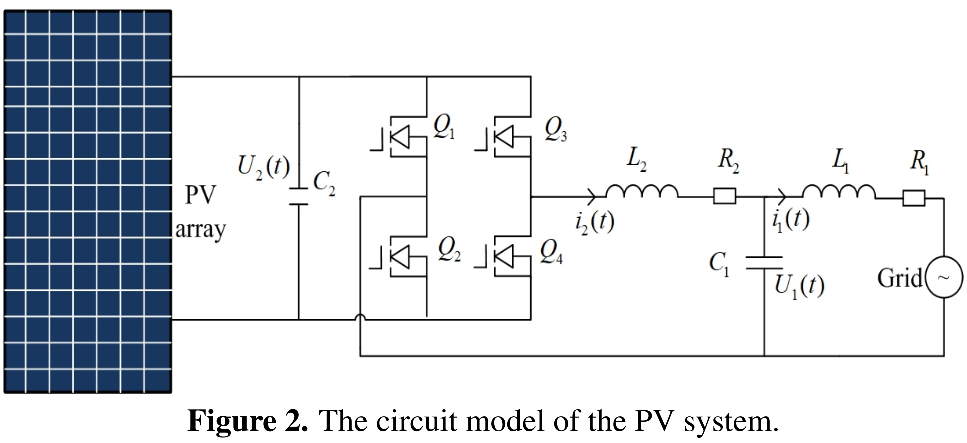

Figure 2. The circuit model of the PV system.

On the basis of theoretical knowledge of the electric circuits, we obtain the following mathematical model:

$$
\begin{aligned}
L_1\frac{di_1(t)}{dt} &= -R_1 i_1(t) - U_g + U_1(t),\\
C_1\frac{dU_1(t)}{dt} &= -i_1(t) + i_2(t),\\
L_2\frac{di_2(t)}{dt} &= U_2(t)D(u) - U_1(t) - R_2 i_2(t),
\end{aligned} \tag{4.1}
$$

where U_g stands for the voltage of the power grid, $i_1(t)$ and $i_2(t)$ are the currents flowing through inductors L_1 and L_2, $U_1(t)$ and $U_2(t)$ are the voltages on both sides of C_1 and C_2, respectively, and $D(u)$ are the duty cycles of the MOS transistors Q_1, Q_2, Q_3, and Q_4. The control input for grid-connected photovoltaic systems is the duty cycle, thus it should be constrained between 0 and 1 in absolute value. Consequently, the side effect of the actuator saturation cannot be overlooked. To eliminate the affect of the symmetric saturated link, the hyperbolic tangent function is adopted in place of the link.

The state variables are defined as $x_1 = i_1(t)$, $x_2 = U_1(t)$, and $x_3 = i_2(t)$. From (2.2) and (2.3), Eq (4.1) is reformulated as

$$
\begin{aligned}
\dot{x}_1 &= -\frac{R_1}{L_1}x_1 + \frac{1}{L_1}x_2 - \frac{1}{L_1}U_g,\\
\dot{x}_2 &= -\frac{1}{C_1}x_1 + \frac{1}{C_1}x_3,\\
\dot{x}_3 &= -\frac{1}{L_2}x_2 - \frac{R_2}{L_2}x_3 + \frac{U_2}{L_2}(u+\rho).
\end{aligned} \tag{4.2}
$$

Furthermore, the equivalent resistance of the inductor varies as the temperature changes under actual running conditions. The equivalent resistance of the inductor is difficult to measure, and the measuring instrument can be damaged easily. Therefore, it is assumed that the equivalent resistances R_1 and R_2 are unknown. On the basis of Lemma 2, we adopt two NNs to approximate the unknown terms $f_1(x_1) = -R_1x_1/L_1$ and $f_3(x_2, x_3) = -x_2/L_2 - R_2x_3/L_2$. The dynamic equation (4.2) can be rewritten as

$$
\begin{aligned}
\dot{x}_1 &= \theta_{f,1}^{*T}\psi_{f,1}(x_1) + \varepsilon_{f,1} + \frac{1}{L_1}x_2 - \frac{1}{L_1}U_g,\\
\dot{x}_2 &= -\frac{1}{C_1}x_1 + \frac{1}{C_1}x_3,\\
\dot{x}_3 &= \theta_{f,3}^{*T}\psi_{f,3}(x_2,x_3) + \varepsilon_{f,3} + \frac{U_2}{L_2}(u+\rho).
\end{aligned} \tag{4.3}
$$

Because only the state x_1 is available, and the states x_2 and x_3 are not directly measured, the states x_2 and x_3 are estimated by devising the NN state observer, which is as follows:

$$
\begin{aligned}
\dot{\hat{x}}_1 &= -\frac{1}{L_1}U_g + \hat{\theta}_{f,1}^{T}\psi_{f,1}(x_1) + \frac{1}{L_1}\hat{x}_2 + k_1(y-\hat{x}_1),\\
\dot{\hat{x}}_2 &= -\frac{1}{C_1}x_1 + \frac{1}{C_1}\hat{x}_3 + k_2(y-\hat{x}_1),\\
\dot{\hat{x}}_3 &= \frac{U_2}{L_2}u + \hat{\theta}_{f,3}^{T}\psi_{f,3}(\hat{x}_2,\hat{x}_3) + k_3(y-\hat{x}_1),\\
\hat{y} &= \hat{x}_1.
\end{aligned} \tag{4.4}
$$

Remark 5. Three sensors will be utilized when the current x_1, the voltage x_2, and the current x_3 are all measured. The data of the voltage x_2 and the current x_3 are derived by constructing the state observer in this paper. Thereby, a current sensor and a voltage sensor can be saved.

The observer gains $k_1 = 2$, $k_2 = 2$, and $k_3 = 2$ are chosen such that matrix A_2 is the Hurwitz. By selecting the matrix $Q_0 = 5I$ and solving Eq (2.10), the following matrix $P > 0$ can be derived:

$$P = \begin{bmatrix} 1.4312 & 4.0593 & -1.0319 \\ 4.0593 & 126.8410 & 16.8560 \\ -1.0319 & 16.8560 & 87.0179 \end{bmatrix}.$$

The parameters of the PV grid-connected power system are given in Table 1.

Table 1. The parameters of the PV system.

Parameters	Instructions	Values
y_r	reference current signal (A)	$30sin\,(100\pi t)$
U_g	grid voltage (V)	$311sin\,(100\pi t)$
R_1	equivalent resistance (Ω)	0.1
L_1	inductor (mH)	11.2
U_2	capacitor voltage (V)	400
C_1	capacitor (uF)	3
R_2	equivalent resistance (Ω)	0.1
L_2	inductor (mH)	5.6

In the simulation, the control system uses eight NNs, all devised to include 3 nodes. The centers are uniformly distributed in the interval $[-1, 1]$, and all the widths are $\varpi_i = 1.3$. Then, the activation functions $\psi_i(x_i)$ $(i = 1, 2, 3)$ of the critic and the actor NNs are designed as

$$\psi_i(x_i) = \exp(-\frac{(\hat{x}_i - (i-2))^2}{1.3^2}).$$

The activation functions $\psi_{f,1}(x_1)$ and $\psi_{f,3}(\hat{x}_2, \hat{x}_3)$ of the observer NN are selected as

$$\psi_{f,1}(x_1) = \exp(-\frac{(x_1 - (i-2))^2}{1.3^2}),$$
$$\psi_{f,3}(\hat{x}_2, \hat{x}_3) = \exp(-\frac{(\hat{x}_2 - (i-2))^2 + (\hat{x}_3 - (i-2))^2}{1.3^2}).$$

The optimal virtual controls $\hat{\alpha}_1$ and $\hat{\alpha}_2$, the first-order auxiliary system, and the actual optimized ET controller $\hat{u}^*$ can be designed as

$$\hat{\alpha}_1 = -\frac{\bar{\eta}_1}{L_1 r_1} z_1 - \frac{1}{2L_1 r_1}\hat{\theta}_{a1}^T \psi_1(z_1),$$
$$\hat{\alpha}_2 = -\frac{\bar{\eta}_2}{C_1 r_2} z_2 - \frac{1}{2C_1 r_2}\hat{\theta}_{a2}^T \psi_2(z_2),$$

$$\dot{\tau}_{sat} = \frac{U_2}{L_2}\bar{\upsilon} - \sigma\tau_{sat},$$
$$\hat{u}^* = -\frac{U_2}{2L_2 r_3}(2z_3\bar{\eta}_3 + \hat{\theta}_{a3}^T\psi_3(z_3)),$$
$$\wp(t) = \hat{u}^*(t) - \widehat{m}\tanh(\frac{z_n\widehat{m}}{\bar{m}}).$$

The parameters of the filter are chosen as $\omega_2 = \omega_3 = 0.001$. The parameters of the ET mechanism are chosen as $\bar{m} = 0.2$, $\widehat{m} > 0.01$, and $\breve{m} = 0.05$. The parameter of the first-order auxiliary subsystem is chosen as $\sigma = 1$. The parameters of the optimal virtual controls $\hat{\alpha}_1$, $\hat{\alpha}_2$, and $\hat{u}^*$ are selected as $r_1 = 1000$, $q_1 = 1$, $\bar{\eta}_1 = 10$, $r_2 = 1600$, $q_2 = 1$, $\bar{\eta}_2 = 0.001$, $r_3 = 0.5$, $q_3 = 0.01$, and $\bar{\eta}_3 = 1$. The parameter of the weight update laws $\hat{\theta}_{f,1}$, $\hat{\theta}_{f,3}$, $\hat{\theta}_{c1}$, $\hat{\theta}_{a1}$, $\hat{\theta}_{c2}$, $\hat{\theta}_{a2}$, $\hat{\theta}_{c3}$, and $\hat{\theta}_{a3}$ are chosen as $b_1 = 5$, $b_3 = 5$, $\eta_1 = 30$, $\eta_3 = 10$, $\beta_{c1} = 0.025$, $\beta_{a1} = 50$, $\beta_{c2} = 0.001$, $\beta_{a2} = 10$, $\beta_{c3} = 1$, and $\beta_{a3} = 0.1$. The initial values of $\hat{\theta}_{f,1}$, $\hat{\theta}_{f,2}$, and $\hat{\theta}_{a1}$ in the simulation are selected as $\hat{\theta}_{f,1} = [1.2, 1.2, 1.2, 1, 1]^T$, $\hat{\theta}_{f,2} = [1.2, 1.2, 1.2, 1.2, 1.9]^T$, and $\hat{\theta}_{a1} = [1.2, 1.2, 1.2, 1.9, 1.9]^T$, and the other initial values are zero. The initial conditions are chosen as $x_1(0) = 0(\mathrm{A})$, $x_2(0) = 0(\mathrm{V})$, $x_3(0) = 0(\mathrm{A})$, $\hat{x}_1(0) = 0.11(\mathrm{A})$, $\hat{x}_2(0) = 0.15(\mathrm{V})$, and $\hat{x}_3(0) = 0.15(\mathrm{A})$. The parameters of the DoS attack model are assumed as $T = 2$, $\tau_D = 0.05$, and $\ell = 0.2$. From Assumptions 2 and 3, $n(0, 0.2) \le 4.2$, $|\Phi(0, 0.2)| \le 0.1\mathrm{s}$. Thus, we set $n(0, 0.2) = 4$ and $|\Phi(0, 0.2)| = 0.08\mathrm{s}$, i.e., in this paper, regarding the frequency of DoS attack, the number of the attacks in this simulation is set to four, which means that four attacks occur within 0.2s. The DoS attack is activated at the time intervals $[0.01\mathrm{s}, 0.03\mathrm{s}] \bigcup [0.06\mathrm{s}, 0.07\mathrm{s}] \bigcup [0.1\mathrm{s}, 0.12\mathrm{s}] \bigcup [0.16\mathrm{s}, 0.19\mathrm{s}]$. The time interval of the DoS attack is represented by the gray shaded portion. Then, as shown in Figures 3–16, the simulation outcomes are displayed. The curves of the 2-norms of the weight vectors of the critic, actor, and observer NNs are shown in Figures 3–5. Figure 6 presents the response curves of the cost function.

Remark 6. The control schemes of the literature [19, 23] can also achieve control of the grid-connection PV power system (4.2). Nevertheless, these control approaches are only able to ensure that all signals in the closed-loop system are bounded. They are unable to realize the optimized control goal, that is, they do not ensure that the cost function is minimized.

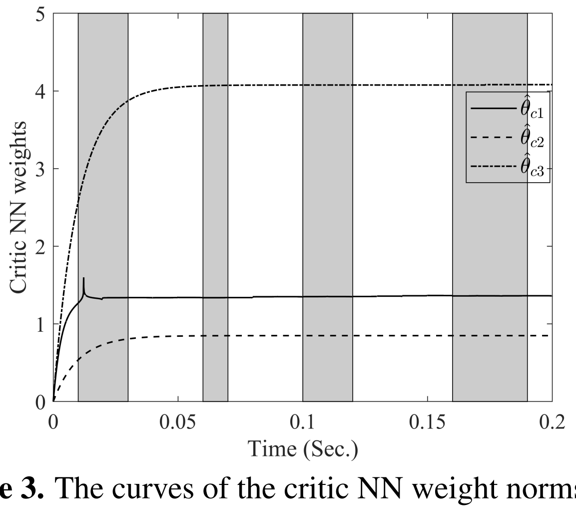

Figure 3. The curves of the critic NN weight norms $\|\hat{\theta}_{ci}\|$.

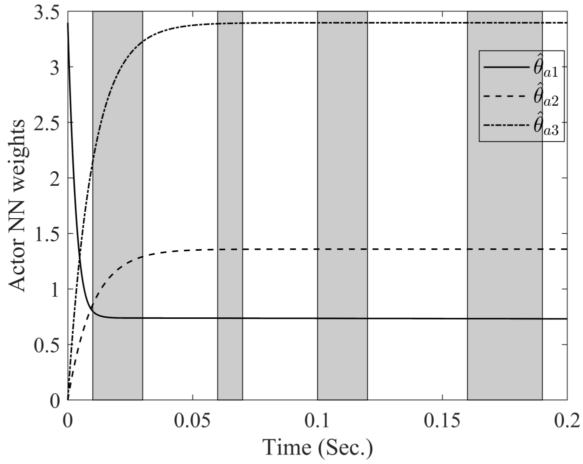

Figure 4. The curves of the actor NN weight norms $\|\hat{\theta}_{ai}\|$.

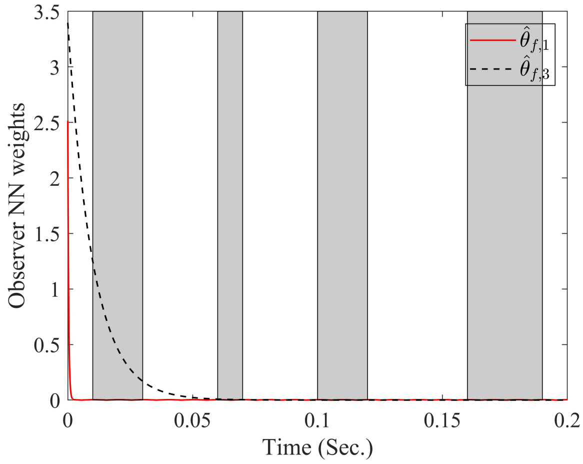

Figure 5. The curves of the observer NN weight norms $\|\hat{\theta}_{f,1}\|$ and $\|\hat{\theta}_{f,3}\|$.

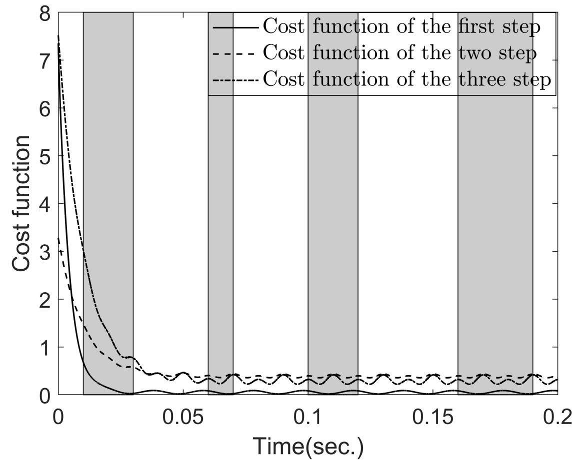

Figure 6. The curves of the cost function.

From Figure 7, it can be seen that the current x_1 can accurately follow the reference current signal y_r under DoS attacks. The state observer estimation curves are plotted in Figures 8–10. Figure 11 shows that the estimation errors of the state variables x_1 (black solid line), x_2 (black dotted line), and x_3 (black dashed line) nearly converge to zero. Figure 12 displays the control input curves. The black dashed line in Figure 12 shows that if the saturated nonlinear link is not considered, the amplitude of the control signal will be larger than -1, exceeding the duty cycle constraints. Nevertheless, this paper investigated the optimized saturated control scheme (red solid line) to ensure that the amplitude of the control signal is between 0 and 1 in absolute value at all times, which satisfies the duty cycle conditions. In addition, when the DoS attack is activated, the actual controller is equal to zero. The interevent times of control input are shown in Figure 13. As shown in Figures 14–16, the comparison outcomes with the corresponding backstepping control strategy in [23] and the similar optimized approaches in [31] and [39] are respectively given. It is observed that the tracking error $x_1 - y_r$ of the developed optimized secure ETC scheme in this paper is much smaller. Accordingly, the proposed NN optimal ETC scheme can achieve superior tracking performance.

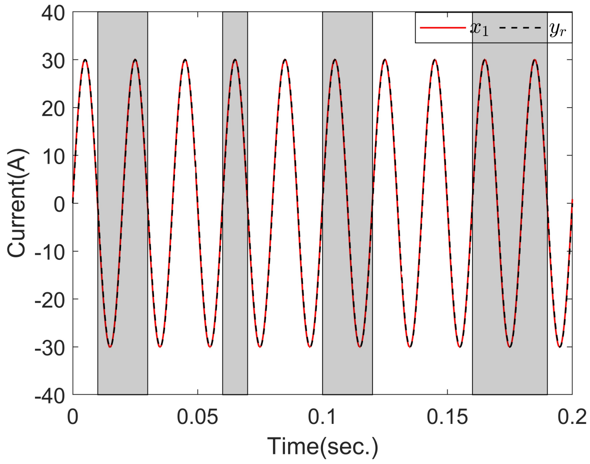

Figure 7. The curves of the current x_1 and reference current signal y_r.

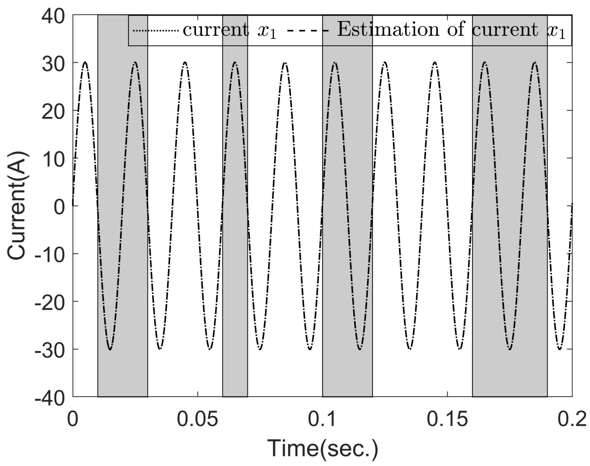

Figure 8. Current x_1 and its estimation curves.

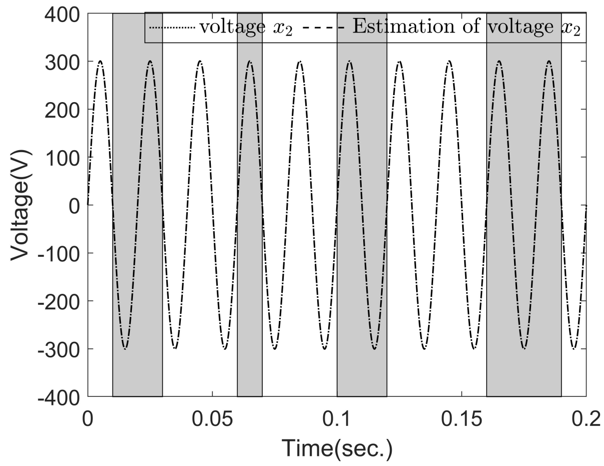

Figure 9. Voltage x_2 and its estimation curves.

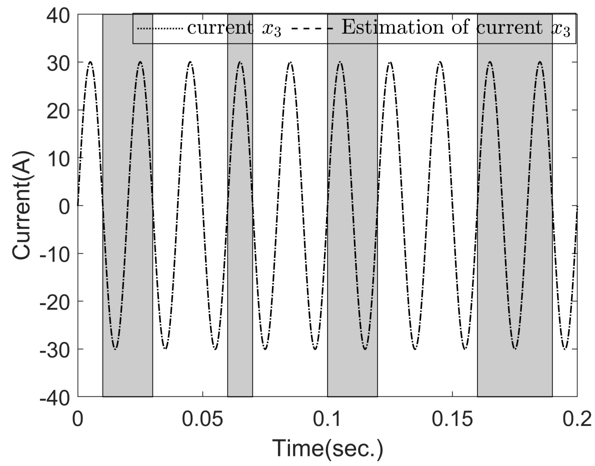

Figure 10. Current x_3 and its estimation curves.

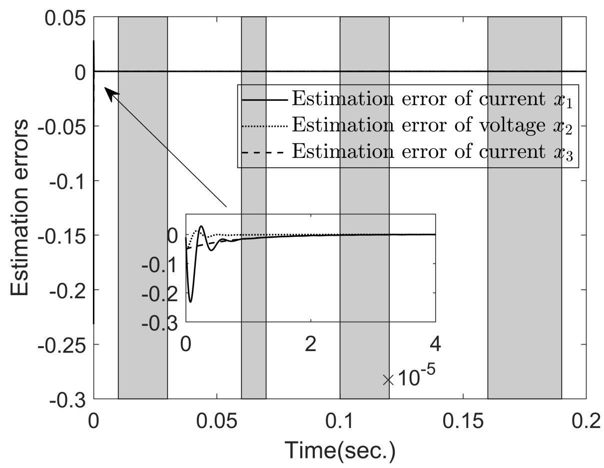

Figure 11. Estimation error curves of the observer.

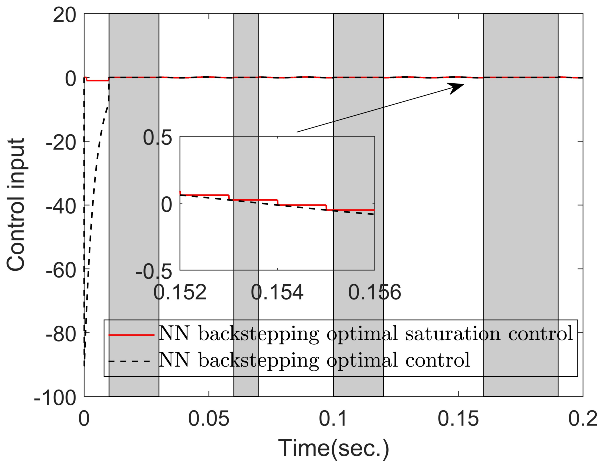

Figure 12. Control input curves.

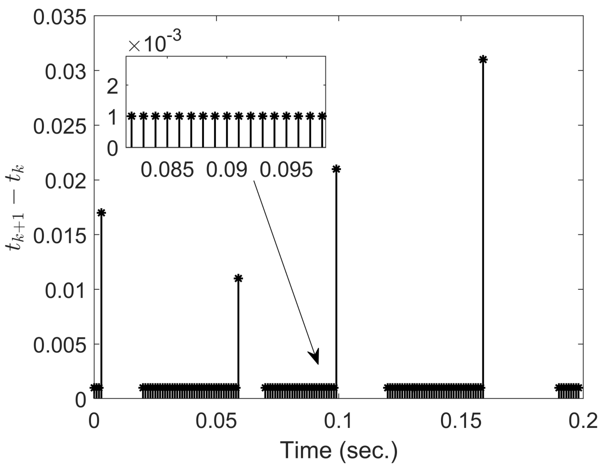

Figure 13. Interevent times of control input.

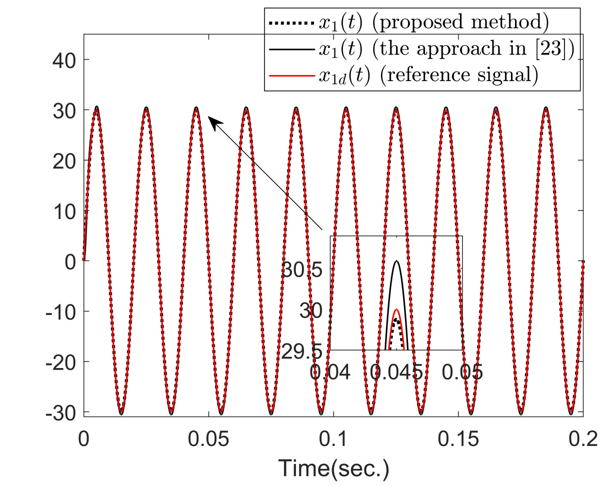

Figure 14. Current x_1 curves by the presented method and in [23].

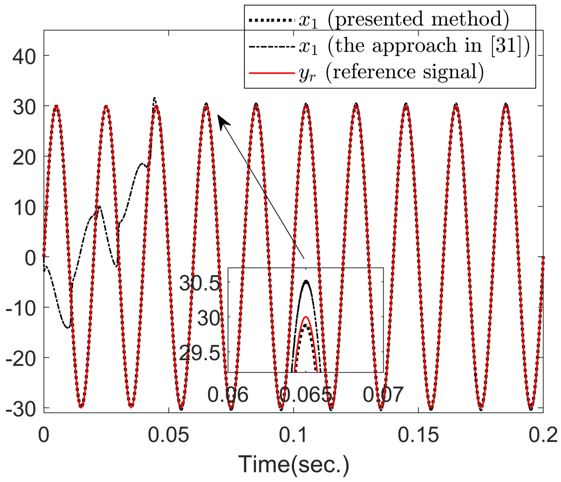

Figure 15. Current x_1 curves by the proposed approach and in [31].

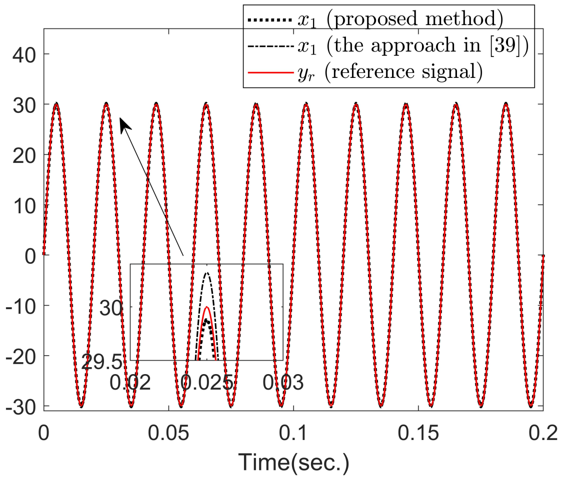

Figure 16. Current x_1 curves by the presented method and in [39].

5. Conclusions

This paper presented an NN adaptive optimization secure output feedback ETC scheme for nonlinear systems with unmodeled dynamics under DoS attacks. The saturation nonlinear link was eliminated by employing the hyperbolic tangent function and an auxiliary subsystem. The observer-critic-actor architecture based on RL was applied in the controller design process to realize the optimal control and minimize the cost function. Furthermore, redundant resource consumption and Zeno behavior can be avoided effectively. The optimal secure control scheme presented in this paper has guaranteed system stability when the optimized controller is subjected to DoS attacks. By utilizing Lyapunov stability theory, it has been proven that all signals of the closed-loop system are SGUUB. Finally, the simulation results of the single-phase PV grid-connected power generation system has been given to further validate the conclusions of the theoretical analysis. Moreover, future research directions will center on the optimal game control problem for uncertain nonlinear systems, while also taking the triggering of the parameter estimator-to-controller channel into consideration.

Author contributions

Jun Hu: Conceptualization, Data curation, Methodology, Writin–review and editing; Wei Liu: Methodology, Conceptualization, Formal analysis, Writing–original draft; Shuai Cheng: Validation, Software, Visualization. All authors have read and approved the final version of the manuscript for publication.

Use of Generative-AI tools declaration

We confirm that AI tools (e.g., ChatGPT/Grammarly) were used solely to improve the English language and readability of the manuscript. The authors take full responsibility for the accuracy and originality of all content. No AI was used to generate data, results, or core scientific conclusions.

Acknowledgments

This work was supported by the Key Research and Development Program of Liaoning Province under Grant No. 2025JH2/102800001.

Conflict of interest

The authors declare no conflict of interest.

References

1. G. Lai, G. Tao, Y. Zhang, Z. Liu, Adaptive control of noncanonical neural-network nonlinear systems with unknown input dead-zone characteristics, *IEEE Trans. Neur. Net. Lear.*, **31** (2020), 3346–3360. https://doi.org/10.1109/tnnls.2019.2943637
2. Y.-J. Liu, W. Zhao, L. Liu, D. Li, S. Tong, C. L. P. Chen, Adaptive neural network control for a class of nonlinear systems with function constraints on states, *IEEE Trans. Neur. Net. Lear.*, **34** (2023), 2732–2741. https://doi.org/10.1109/tnnls.2021.3107600
3. K. Li, X. Liu, Fuzzy adaptive cooperative prescribed time control for nonlinear vehicular platoon systems, *IEEE Trans. Fuzzy Syst.*, **33** (2025), 1568–1577. https://doi.org/10.1109/tfuzz.2025.3528399
4. Y. Gao, W. Sun, X. Xie, Adaptive fuzzy prescribed-time control of high-order nonlinear systems with actuator faults, *Inform. Sciences*, **667** (2024), 120484. https://doi.org/10.1016/j.ins.2024.120484
5. K. Feng, K. Li, Y. Li, Dynamic event-based predefined-time adaptive fuzzy trajectory tracking control of underwater tracked robot with specified accuracy, *IEEE Trans. Autom. Sci. Eng.*, **23** (2026), 10281–10295. https://doi.org/10.1109/tase.2026.3694398
6. S. Tong, Y. Li, S. Sui, Adaptive fuzzy tracking control design for SISO uncertain nonstrict feedback nonlinear systems, *IEEE Trans. Fuzzy Syst.*, **24** (2016), 1441–1454. https://doi.org/10.1109/tfuzz.2016.2540058

7. S. Wang, J. Xia, W. Sun, H. Shen, H. Zhang, Observer-based adaptive event-triggered tracking control for nonlinear MIMO systems based on neural networks technique, *Neurocomputing*, **433** (2021), 71–82. https://doi.org/10.1016/j.neucom.2020.12.050
8. Y. Li, K. Li, S. Tong, An observer-based fuzzy adaptive consensus control method for nonlinear multiagent systems, *IEEE Trans. Fuzzy Syst.*, **30** (2022), 4667–4678. https://doi.org/10.1109/tfuzz.2022.3154433
9. D. Ye, T. Zhang, Summation detector for false data-injection attack in cyber-physical systems, *IEEE Trans. Cybernetics*, **50** (2020), 2338–2345. https://doi.org/10.1109/tcyb.2019.2915124
10. K. Dong, G. Yang, H. Wang, Estimator-based event-triggered output synchronization for heterogeneous multi-agent systems under denial-of-service attacks and actuator faults, *Inform. Sciences*, **657** (2024), 119955. https://doi.org/10.1016/j.ins.2023.119955
11. X. Liu, K. Shi, H. Yan, J. Cheng, S. Wen, Integral-based event-triggering switched LFC scheme for power system under deception attack, *Expert Syst. Appl.*, **234** (2023), 121075. https://doi.org/10.1016/j.eswa.2023.121075
12. W. He, Y. Shi, Y. Wang, Adaptive resilient control for a class of strict-feedback nonlinear systems under replay attacks, *IFAC-PapersOnLine*, **58** (2024), 514–519. https://doi.org/10.1016/j.ifacol.2024.07.270
13. J. Zhao, G.-H. Yang, An observer-based resilient control method against intermittent DoS attacks for nonstrict-feedback nonlinear cyberphysical systems with tracking errors constraint, *Int. J. Fuzzy Syst.*, **26** (2024), 596–612. https://doi.org/10.1007/s40815-023-01619-6
14. X. Shao, D. Ye, Neural-network-based adaptive secure control for nonstrict-feedback nonlinear interconnected systems under DoS attacks, *Neurocomputing*, **448** (2021), 263–275. https://doi.org/10.1016/j.neucom.2021.03.087
15. L. Zou, X. Liu, Robust adaptive control for a class of networked nonlinear systems under denial-of-service attacks, *Nonlinear Dyn.*, **111** (2023), 1385–1398. https://doi.org/10.1007/s11071-022-07901-w
16. Y. Xu, S. Chai, P. Shi, B. Zhang, Y. Wang, Resilient and event-triggered control of stochastic jump systems under deception and denial of service attacks, *Int. J. Robust Nonlin.*, **33** (2023), 1821–1837. https://doi.org/10.1002/rnc.6463
17. H. Zhou, S. Tong, Fuzzy adaptive resilient formation control for nonlinear multiagent systems subject to DoS attacks, *IEEE Trans. Fuzzy Syst.*, **32** (2024), 1446–1454. https://doi.org/10.1109/tfuzz.2023.3327140
18. H. Zhang, Y. Li, K. Li, Event-triggered based adaptive finite-time enclosed control for multirobot systems via bearing information, *Int. J. Robust Nonlin.*, **36** (2026), 5291–5305. https://doi.org/10.1002/rnc.70513
19. T. Wang, X. Zhang, Y. Li, Type-2 fuzzy adaptive event-triggered saturation control for photovoltaic grid-connected power systems, *Int. J. Fuzzy Syst.*, **23** (2021), 1150–1162. https://doi.org/10.1007/s40815-021-01078-x
20. C. Yang, D. Huang, W. He, L. Cheng, Neural control of robot manipulators with trajectory tracking constraints and input saturation, *IEEE Trans. Neur. Net. Lear.*, **32** (2021), 4231–4242. https://doi.org/10.1109/tnnls.2020.3017202

21. T. Wang, H. Zhang, S. Sui, Observer-based adaptive neural network event-triggered quantized control for active suspensions with actuator saturation, *Neurocomputing*, **614** (2025), 128770. https://doi.org/10.1016/j.neucom.2024.128770
22. Z. Gao, Y. Zhang, G. Guo, Adaptive fixed-time sliding mode control of vehicular platoons with asymmetric actuator saturation, *IEEE Trans. Veh. Technol.*, **72** (2023), 8409–8423. https://doi.org/10.1109/tvt.2023.3247608
23. T. Wang, X. Zhang, Y. Li, Type-2 fuzzy adaptive output feedback saturation control for photovoltaic grid-connected power systems, *Int. J. Control Autom. Syst.*, **19** (2021), 2759–2768. https://doi.org/10.1007/s12555-020-0629-9
24. Y. Li, S. Tong, T. Li, Composite adaptive fuzzy output feedback control design for uncertain nonlinear strict-feedback systems with input saturation, *IEEE Trans. Cybernetics*, **45** (2015), 2299–2308. https://doi.org/10.1109/tcyb.2014.2370645
25. J. Ma, S. Ge, Z. Zheng, D. Hu, Adaptive NN control of a class of nonlinear systems with asymmetric saturation actuators, *IEEE Trans. Neur. Net. Lear.*, **26** (2015), 1532–1538. https://doi.org/10.1109/tnnls.2014.2344019
26. C. Wen, J. Zhou, Z. Liu, H. Su, Robust adaptive control of uncertain nonlinear systems in the presence of input saturation and external disturbance, *IEEE Trans. Autom. Contr.*, **56** (2011), 1672–1678. https://doi.org/10.1109/tac.2011.2122730
27. W. Sun, S. Diao, S. Su, Z. Sun, Fixed-time adaptive neural network control for nonlinear systems with input saturation, *IEEE Trans. Neur. Net. Lear.*, **34** (2023), 1911–1920. https://doi.org/10.1109/tnnls.2021.3105664
28. H. Zhang, X. Zhao, H. Wang, B. Niu, N. Xu, Adaptive tracking control for output-constrained switched MIMO pure-feedback nonlinear systems with input saturation, *J. Syst. Sci. Complex.*, **36** (2023), 960–984. https://doi.org/10.1007/s11424-023-1455-y
29. X. Fang, H. Fan, W. Wang, L. Liu, B. Wang, Z. Cheng, Adaptive finite-time fault-tolerant control of uncertain systems with input saturation, *IEEE Trans. Syst. Man Cyber. A*, **53** (2023), 165–177. https://doi.org/10.1109/tsmc.2022.3170573
30. H. Zhang, T. Wang, T. Zhang, Adaptive neural network output feedback optimal saturation control for single-phase photovoltaic grid-connected power systems, *Int. J. Adapt. Control*, in press. https://doi.org/10.1002/acs.70107
31. G. Wen, S. Ge, C. L. P. Chen, F. Tu, S. Wang, Adaptive tracking control of surface vessel using optimized backstepping technique, *IEEE Trans. Cybernetics*, **49** (2018), 3420–3431. https://doi.org/10.1109/tcyb.2018.2844177
32. K. Li, Y. Li, Fuzzy adaptive optimization prescribed performance control for nonlinear vehicle platoon, *IEEE Trans. Fuzzy Syst.*, **32** (2024), 360–372. https://doi.org/10.1109/tfuzz.2023.3298385
33. H. Shen, W. Zhao, J. Cao, J. H. Park, J. Wang, Predefined-time event-triggered tracking control for nonlinear servo systems: a fuzzy weight-based reinforcement learning scheme, *IEEE Trans. Fuzzy Syst.*, **32** (2024), 4557–4569. https://doi.org/10.1109/tfuzz.2024.3403917
34. H. Shen, X. Yu, H. Yan, J. H. Park, J. Wang, Robust fixed-time sliding mode attitude control for a 2-DOF helicopter subject to input saturation and prescribed performance, *IEEE Trans. Transp. Electr.*, **11** (2025), 1223–1233. https://doi.org/10.1109/tte.2024.3402316

35. Y. Li, Y. Xu, K. Li, Dynamic event-triggered optimal control for heterogeneous vehicle platoon based on integral reinforcement learning, *IEEE Trans. Netw. Sci. Eng.*, **12** (2025), 1885–1897. https://doi.org/10.1109/tnse.2025.3540993
36. K. Li, Y. Xu, Y. Li, Data-based event-triggered cooperative optimal output regulation of nonlinear multiagent systems, *IEEE Trans. Syst. Man Cyber. A*, **55** (2025), 6273–6284. https://doi.org/10.1109/tsmc.2025.3577375
37. K. Sun, Y. Li, S. Tong, Fuzzy adaptive output feedback optimal control design for strict-feedback nonlinear systems, *IEEE Trans. Syst. Man Cyber. A*, **47** (2017), 33–44. https://doi.org/10.1109/tsmc.2016.2586193
38. H. Zhang, L. Cui, X. Zhang, Y. Luo, Data-driven robust approximate optimal tracking control for unknown general nonlinear systems using adaptive dynamic programming method, *IEEE Trans. Neural Networ.*, **22** (2011), 2226–2236. https://doi.org/10.1109/tnn.2011.2168538
39. T. Zhang, H. Xu, Adaptive optimal dynamic surface control of strict-feedback nonlinear systems with output constraints, *Int. J. Robust Nonlin.*, **30** (2020), 2059–2078. https://doi.org/10.1002/rnc.4864
40. K. Li, Y. Li, Fuzzy adaptive optimal consensus fault-tolerant control for stochastic nonlinear multiagent systems, *IEEE Trans. Fuzzy Syst.*, **30** (2022), 2870–2885. https://doi.org/10.1109/tfuzz.2021.3094716

AIMS Press